TAMPEREEN TEKNILLINEN YLIOPISTO
TAMPERE UNIVERSITY OF TECHNOLOGY

ZHU WEIJIE

PERFORMANCE ANALYSIS OF ASYNCHRONOUS NB-IOT UPLINK SYSTEMS

Master of Science Thesis

Examiner: prof. Markku Renfors
Examiner and topic approved by the Faculty Council of the Faculty of Computing and Electrical Engineering on 9th August 2017

ABSTRACT

ZHU WEIJIE: Performance Analysis of Asynchronous NB-IoT Uplink Systems
Tampere University of technology
Master of Science Thesis, 68 pages
October 2017
Master's Degree Programme Electrical Engineering
Major: Wireless Communication
Examiner: Professor Markku Renfors

Keywords: NB-IoT, LTE, 5G, windowing, filtering, power amplifier, asynchronous

The Third Generation Partnership Project (3GPP) published LTE release 13, which standardized a new radio access network (RAN) called Narrowband Internet of Things (NB-IoT). Such networks, particularly designed for massive machine-type communications (mMTC), inherit theIR functionalities from the existing LTE systems with slight differences and operate in a narrow frequency band of 180 kHz, consisting of one resource block (RB) of 12 LTE subcarriers.

This thesis is mainly focused on single-tone in-band transmission with one 15 kHz subcarrier of the NB-IoT RB in the middle of the LTE RBs. The aim of this thesis is to examine the performance of both NB-IoT transmission and LTE transmission after certain enhancements of the NB-IoT transmitter. These additional approaches including time-domain windowing and filtering. Also a nonlinear power amplifier model for the NB-IoT transmitter is included in the study. It is worth to mention that NB-IoT and LTE signals are transmitted together through asynchronous channels to evaluate the effect of noise and Inter-Carrier Interference (ICI). In order to compare the effects of different modulation schemes, 4-QAM and 64-QAM are both considered for LTE transmission. Filters are designed to suppress the spectral sidelobes of transmitted signals to reduce the interferences due to asynchronous operation. What's more, transmissions with one-subcarrier-wide guard band between the active NB-IoT and LTE subcarriers or without guard band are both examined from bit error-rate (BER) perspective.

PREFACE

I would like to express my greatly appreciation to a number of people; without their support and contribution, this journey of studies and work might not have been possible.

First of all, I would like to express my sincere gratitude to my survivor, Prof. Markku Renfors, for his selfless help and guidance from time to time, in achieving the production of this thesis. His patience and time spent in helping me is priceless.

I would like to thank my parents for their support and encouragement throughout my whole studying period in Finland. Through the whole journey, they always stay with me and give me advices when necessary. Thanks to my beloved friend Guo Mingfeng that accompany with me every day and night. Thanks to my roommate, Fan Yuchuan.

CONTENT

LIST OF FIGURES

LIST OF TABLES

LIST OF SYMBOLS AND ABBREVIATIONS

3GPP	The third Generation Partnership Project
4G	Fourth-Generation
5G	Fifth Generation
AST	Adaptive Symbol Transition
AWGN	Additional White Gaussian Noise
BER	Bit Error Ratio
BO	Back-Off
BPSK	Binary Phase Shift Keying
CE-OFDM	Constant Envelop OFDM
CC	Cancellation Carriers
CFO	Carrier Frequency Offset
CP	Cyclic Prefix
DC	Direct Current
DRX	Discontinuous Reception
eMBB	Enhanced Mobile Broad-Band
FDMA	Frequency Division Multiple Access
FFT	Fast Fourier Transform
GI	Guard Interval
GSM	Global System for Mobile Communication
IDFT	Inverse Discrete Fourier Transform
IFFT	Inverse Fast Fourier Transform
IMT	International Mobile Telecommunication
ITU-R	International Telecommunication Union Radiocommunication Sector
LPWA	Low Power Wide Area
LTE	Long Term Evolution
M2M	Machine to Machine
MCS	Multi-Choice Sequences
mMTC	Massive Machine Type Communication
NB-IoT	Narrow Band Internet of Things
OFDM	Orthogonal Frequency Division Multiplexing
PA	Power Amplifier
PAPR	Peak-to-Average-Power Ratio
QAM	Quadrature Amplitude Modulation
RAN	Radio Access Network
RB	Resource Block
RRC	Root Raised Cosine
SIM	Subscriber Identity Module
SNR	Signal to Noise Ratio

SW	Subcarrier Weighting
TOF	Timing Offset
URLLC	Ultra-Reliable and Low Latency Communication
V2X	Vehicle to Everything
WLAN	Wireless Local Area Network
WP	Working Party

1. INTRODUCTION

In modern wireless communications, the existing long-term evolution-advanced (LTE-A) system cannot fulfill the increasing requirements from multiple usage scenarios. This has resulted in new research and standardization activities on developing a new standard for fifth-generation (5G) cellular networks. Meanwhile, the Third Generation Partnership Project (3GPP) introduced a new radio access network to the LTE family in Release 13, which is named as Narrow Band Internet of Things (NB-IoT) [1]. NB-IoT is considered as a communication system that is capable of connecting billions of devices with a great range of applications ranging from environment monitoring, utilities, and logistics to various industrial fields. One of the possible deployment scenarios of NB-IoT is to operate in narrow frequency bands within existing LTE systems. This is essential for reducing the deployment budget and improve the spectrum utilization efficiency. NB-IoT is expected to be reused, with some enhancements, for massive Machine Type Communication (mMTC) in the 5G system.

In this context, several drawbacks should be considered since both NB-IoT and uplink LTE are using the orthogonal frequency-division multiplexing (OFDM) scheme. One of the major problems of OFDM is spectral leakage. OFDM subcarriers have high sidelobes around activated subcarriers, which may lead to high interference to adjacent users [2]. Especially, NB-IoT subcarriers are allocated close to LTE Resource Blocks (RBs) with different transmitted power levels. Both signals could have a possibility to leak high interference to adjacent subcarriers, unless the two systems are perfectly synchronized, which might not be the case in practical operation.

Consequently, plenty of approaches have been studied to reducing the sidelobe of OFDM signals. A straightforward way is to use filters, but this can increase system complexity and introduce extensive delays [3]. Other proposed methods include the use of interference cancellation carriers (CC) [4][5], subcarrier weighting (SW) [6], multi-choice sequences (MCS) [7], and Adaptive Symbol Transition (AST) [8]. Although these techniques can reduce the sidelobes significantly, they require relatively high computational complexity.. In contrast, time domain windowing is much simpler by using guard intervals on both sides of each transmitted OFDM symbol.

In this thesis, time domain windowing is implemented in single-tone NB-IoT transmission to demonstrate its capability to reduce interference leakage. Both NB-IoT and LTE transmission chains are simulated together to evaluate the interference leakage in practical case study using a 1.4 MHz LTE system scenario where the NB-IoT device's uplink transmission is not synchronized to the LTE network. What's more, the effect of NB-IoT device's power amplifier's nonlinear characteristic on the interference leakage is investigated. The BER performances of both NB-IoT and LTE are evaluated with different windowed cyclic prefix (CP) extension schemes, different power amplifier's (PA) back-off (BO) values, and relative power levels of NB-IoT and LTE transmissions.

The structure of this thesis is as follows: Chapter 2 illustrates the development and scenarios of 5G and NB-IoT. Chapter 3 elaborates the model of basic OFDM system which is used in this thesis. Chapter 4 develops the mathematic model of NB-IoT, considering especially the features of windowing. Filtering and power amplifier modeling are also explained in detail for the considered cases. Furthermore, a novel phase rotation scheme for NB-IoT is presented to maintain the constant envelope characteristic of the $\pi/2$-BPSK modulation after windowing. Chapter 5 focuses on the analysis of the proposed system which is based on the 1.4 MHz LTE scenario. The effects of windowing, filtering, and power amplifier are examined from the spectrum perspective. Various CP-extension schemes for windowing are considered and BO values for PA are selected for simulations. What's more, different practical test cases regarding the relative power levels of NB-IoT and LTE signals at the base station receiver are defined to examine the different usage scenarios in practice. Detailed comparative figures show the properties of proposed approach in terms of BER performance and sidelobe suppression capability. Chapter 6 summarizes the conclusions obtained by simulations and discusses possible future research topics.

2. 5G AND NB-IOT

With increased demands on seamlessly connected society, the maturing Fourth-Generation (4G) communication system seems not capable enough to fulfill explosive growth of mobile internet and different service requirements. This has motivated the development of 5G system concept and related technologies in both academic and industrial communities, with the vision to bring together individuals along with things, applications, transport systems, and even smart cities into a connected network.

According to different application scenarios and user requirements, 5G communication network requires a compatibility across pre-existing technologies and therefore, part of key technologies will be inherited from the LTE-Advanced system. Hence, the potential benefits and reuse of existing LTE/LTE-A ecosystems are maximized.

2.1 5G

2.1.1 5G standardization

International Telecommunication Union's Radiocommunication Sector (ITU-R) endorsed 'IMT for 2020 and beyond' program in early 2012, setting the visions and goals for the development of 5G research activities all over the world. Various organizations and research associations have been involved in launching several programs aiming at key technologies for 5G. While at the same time, the standardization for 5G has to be approved by ITU-R [10]. Its Working Party (WP) 5D has a leading role in standardization, and it is currently preparing the details of performance requirements, evaluation criteria and methodology for the evaluation of candidate technologies.

In this context, in 2015, the Third Generation Partnership Project (3GPP) has also published a timeframe for 5G which aligns with ITU-R for standardization of the next generation cellular network, and is shown in Figure 2-1. 3GPP publishes releases once per year and now it has shifted the focus on Release 15 to deliver the first set of 5G standards [11]. The development of 5G technology will be separated into two phases to

finish the primary specifications to allow deployments according to 2020 timeline [11]. Phase 1 will be completed by 2018 in Release 15. Phase 2 will extend the functionalities of 5G to support more services, scenarios and also higher frequency bands. It is planned to be brought out in Release 16 around 2020.

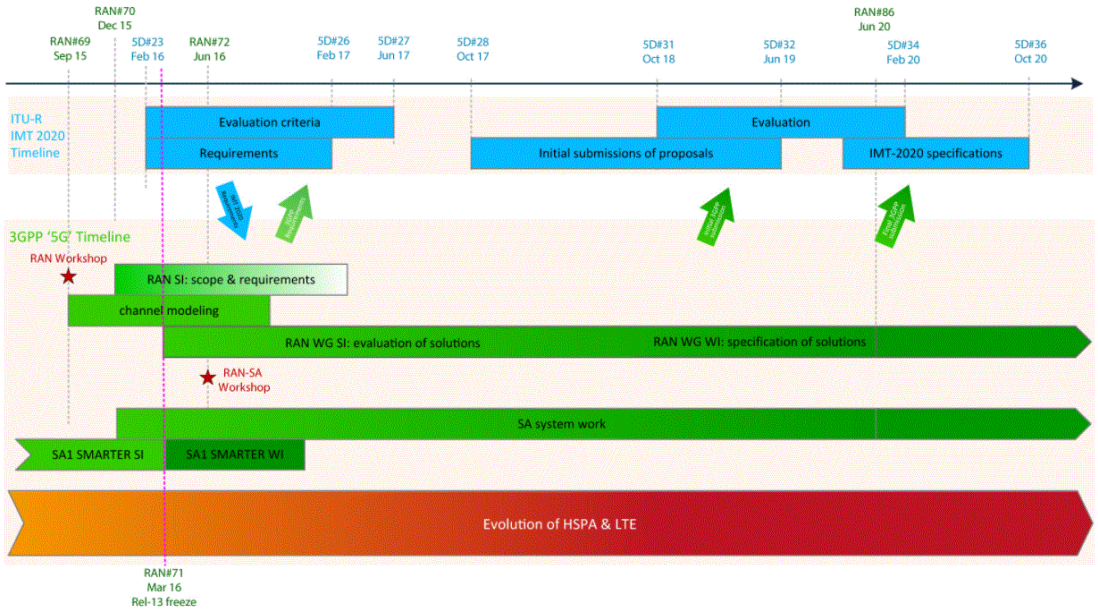

Figure 2-1 *The 3GPP timeline for Next Generation Cellular*
[http://www.3gpp.org/news-events/3gpp-news/1674-timeline_5g]

2.1.2 5G Scenarios

The usage of 5G will not only served for mobile communications. In fact, IMT 2020 is expected to support various usage cases in three categories:

- Enhanced mobile broadband (eMBB): This refers to a communication system that is based on the existing LTE-A but with improved user experience. New technologies will be introduced to support a range of cases, including wide area coverage and hotspots. For the wide area coverage, because of the requirement for seamless coverage and high mobility, transmitter data rates will be increased compared to those provided today. For hotspots, the main scene is with high UE density and high traffic capacity, but less requirement on mobility.

- Ultra-reliable and low latency communications (URLLC): The requirements for URLLC in reliability, latency, and capacity are extremely stringent in all these three applications. Usage cases include Tactile Internet [13], smart city, vehicle-to-everything (V2X), intelligent transportation, and wireless control of industrial manufacturing, etc.

- Massive machine type communications (mMTC): mMTC application is mainly considered as a very large number of electrical devices with low transmission times and low data rates. Devices are required to have very long battery life with low fixed cost.

2.1.3 5G requirements

Towards a system concept, the requirements of 5G is to develop a technical solution that support:

- 10-100 times higher data speed compared to the existing LTE network, reaching 1 to 10 Gbps connections

- 1 millisecond end-to-end round-trip latency

- 1000 times higher data capacity per area [14]

- 10 to 100 times connected devices

- 90 percent reduction in network power consumption

- Up to 10 years battery life for mMTC.

These requirements shall be fulfilled at similar cost as today but based on corresponding scenarios [19].

2.2 NB-IoT

The Internet of Things is revolutionizing the whole society no matter the lifestyle or industrial area and is expected to create steady growth in economy. In this technology-based society, all devices that benefit from an internet connection will eventually be connected. There are more than 16 billion IoT devices worldwide in 2017, and Ericsson

predicted that the total number will be rapidly increased to 28 billion by 2021, half of which will be connected to Machine-to-Machine (M2M) and consumer-electronic devices [15].

M2M or Machine-type-Communications (MTC) plays a significant role as the key sight of IoT deployments. Massive MTC refers to a use case in which thousands of devices seldom transmit and/or receive a small amount of data packets [1]. As a result, low power consumption, low complexity, stability, and long coverage become primary requirements for massive MTC. Especially from the power consumption perspective, the battery of these devices are expected to have up to 10 years of lifetime. As such, in recent years, Low Power Wide Area (LPWA) technologies have been developed to fulfil the great demands of the market. Technologies, such as LoRa and Sigfox, have become extraordinary popular for massive MTC. LoRa and Sigfox are designed to be deployed at an unlicensed spectrum, which is also allocated for Industrial, Scientific and Medical (ISM) applications. Both technologies can support thousands of connections with a coverage distance reaching 10 km. However, the drawback is apparent. Due to commonality of frequency resources in unlicensed spectrum, certain technologies, such as frequency hopping, are considered to prevent coexisting systems from interference, such as Wireless Local Area Network (WLAN) and Bluetooth

Thus, in order to provide a satisfying capacity for massive MTC, another solution is look into the licensed spectrum. Licensed bands do not suffer from un-coordinated co-channel interference from external systems. However, in the uplink the transmission the power is limited, while the downlink budget can be increased due to higher transmission power of base stations.

The Third Generation Partnership Project (3GPP) published LTE release 13, which standardized a new radio access network (RAN) called narrowband Internet of things (NB-IoT). This network inherits the functionalities of existing LTE systems with small differences and operates in a narrow band of 180 kHz, i.e., 12 sub-carriers, and it is particularly designed for massive MTC communications. With upgrade in terms of core network, the existing LTE systems can directly support NB-IoT applications. This is paramount to determine a new radio access into commercial application and plays an essential part in reducing the deployment costs.

The main benefits are obvious: less complexity, lower power consumption, less cost in implementation and larger coverage because of increased transmitted power spectral

density (PSD). The transmission is based on Discontinuous Reception (DRX), which ensure devices to sleep at most of time, and only wake up when necessary to listening to incoming data packets from the network [16]. The Sleep-to-Listen Scheme can, to a significant extent, reduce the complexity as well as the power consumption for the NB-IoT networks [17], especially when the communication would only take place a few thousands of times per year with only few bits of data in each transmission. Thus, a single NB-IoT carrier can support thousands of connections and this can be scaled up once multiple carriers are introduced to the network.

According to Release 13, one additional requirements for NB-IoT is the possibility to deploy it in the 200kHz channel bandwidth of the Global System for Mobile Communications (GSM). As a result, it delivers an effective narrowband operation with 180 kHz bandwidth in uplink and 180 kHz in downlink with frequency-division duplex, which is equivalent to the physical resource block in LTE. This indicates that NB-IoT can be transmitted with LTE signal together in the same carrier. There are three different models for operating NB-IoT signals, as illustrated in Figure 2-2:

Standalone operation: Standalone operation refers to a NB-IoT single which is deployed with one or more existing or re-farmed GSM carriers.

I*n-band operation:* An in-band deployment within existing LTE carriers uses one or a few PRBs of the LTE carrier.

Guard-band operation: Resource blocks with LTE carrier's guard band are allocated and NB-IoT cell is served by the same base station. Compared to in-band operation, less interference is introduced as NB-IoT is only located at one side of LTE carries and with a guard band in-between. At same time, the spectrum utilization efficiency is increased.

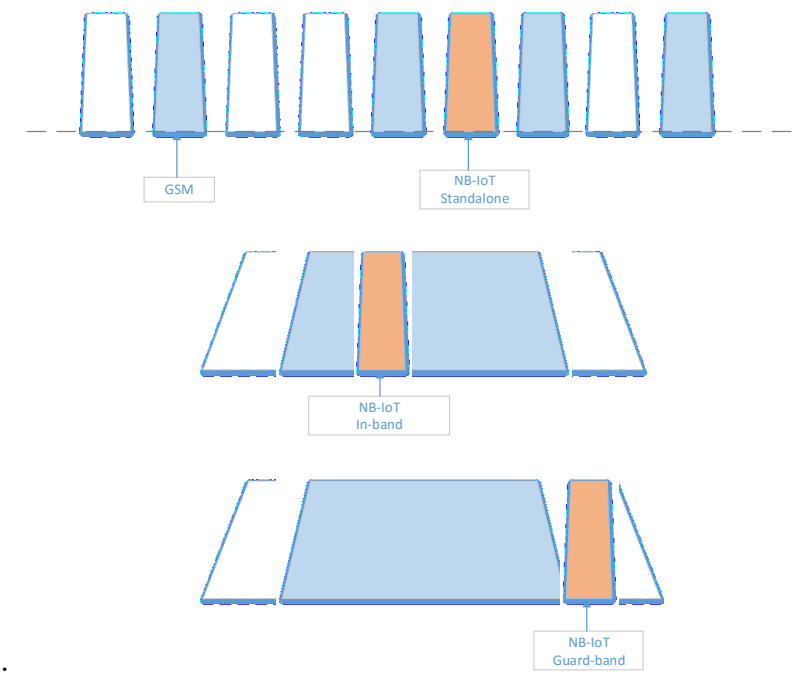

Figure 2-2 *NB-IoT Operation Modes*

2.3 NB-IoT applications

The application environment of mMTC includes but is not limited to environmental monitoring, smart city, smart home, and smart architecture, etc.

2.3.1 Smart metering

Smart metering is one use case of smart home that helps save manpower by remotely collecting electricity, water, and gas meter data over cellular networks [18]. The cost of manual meter reading, and maintenance of meter equipment will consequently be reduced as these two are considered as major cost drivers for conventional metering.

2.3.2 Alarms & Event Detectors

Home safety of human living is also a significant aspect of smart house. Multiple sensors will detect and then report the house status consecutively, especially for home intrusion or emergence situations. Both alarm and events detectors will make use of

sensors that are placed in ideal locations that constantly communicate through LPWA networks.

2.3.3 Smart bicycle

In the past two years, smart bicycle rental has become popular in many cities and are increasingly becoming a lucrative industry as an additional public transportation option. Both the bike rental company and costumers can benefit a lot from both-way communications. A M2M device with SIM card can be embedded into the bike's frame to help locating it. The company won't concern whether the bike will be stolen and from the costumer's perspective, it is easier to find a free bike through integrated mobile application or relative websites.

3. OFDM BASICS

OFDM is a multicarrier modulation scheme that divides the input data stream into many parts to be transmitted in a (typically high) number of narrow subcarriers. Each transmitted OFDM symbol contains certain orthogonal subcarriers. The subcarrier spacing is carefully selected such that each carrier is located on adjacent subcarrier's zero crossing points, as can be seen in Figure 3-1. Although there is overlap in frequency domain, the orthogonality still ensures the transmitted subcarrier signals can be separated from each other in the receiver. Thus, the overlapping of subcarriers provides better spectral efficiency than basic non-overlapping Frequency Division Multiple-Access (FDMA) systems[20].

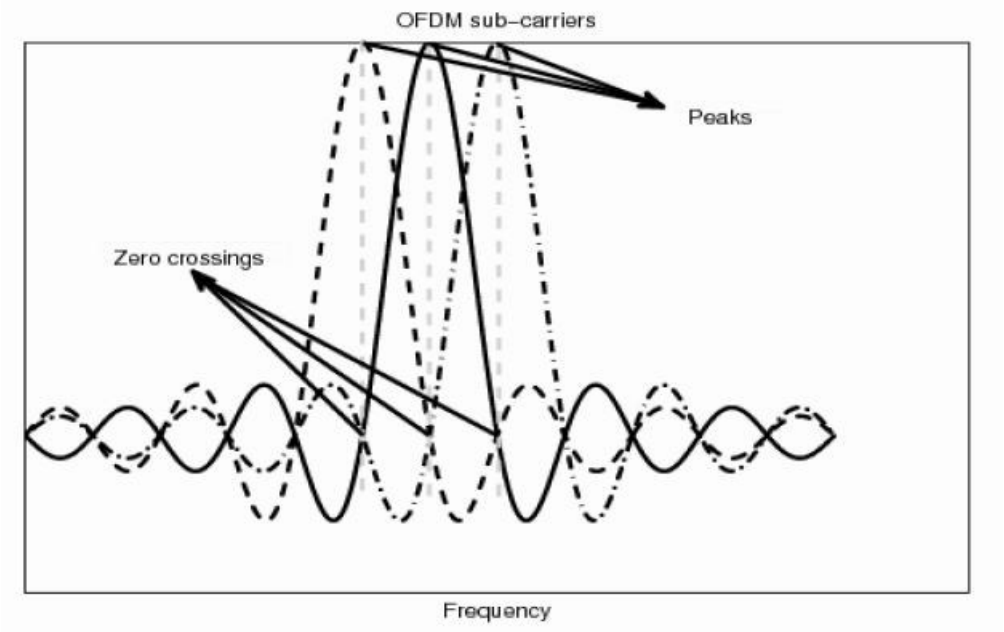

Figure 3-1 *Spectrum of OFDM that consist of several subcarriers*

On the other hand, the subcarriers of OFDM can be considered as a flat fading, which enables to overcome the multipath fading effects in mobile communications. It has high spectrum efficiency and lower distortion; all of which leads to simplified processing at the receiver. These are the main advantages of OFDM.

However, the performance of OFDM relies on the transmission system's linearity and synchronization [23]. Extra symbol timing and frequency-offset control is necessary to

ensure that different uplink users' subcarriers remain orthogonal when arriving at the receiver. Otherwise, the so-called inter-carrier interference (ICI) will affect the whole subcarrier sequences, leading to a huge bit error probability.

Another disadvantage is that an OFDM signal has a relatively large dynamic range of amplitude variation, or in other word, high Peak to Average Power Ratio (PAPR). This impacts the RF amplifier's efficiency as the amplifier needs to be linear while accommodating the large variations. This reduces their power efficiency and makes the power amplifier design as one of the most challenging aspects in the development of mobile devices [22].

3.1 OFDM System Overview

OFDM based transmission and reception system is illustrated in Figure 3-2.

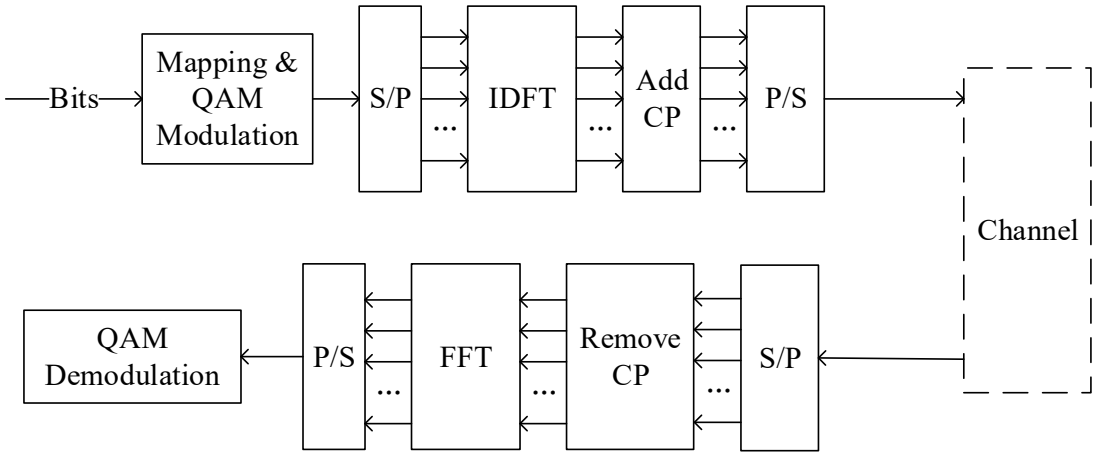

Figure 3-2: *Transmission and reception chain of OFDM system*

3.1.1 QAM and symbol mapping

In modern communication systems, digital modulation can be considered as a priority option. QAM modulation is one of digital modulation techniques that improves the noise resistance compared to analog or time continuous modulation. In OFDM systems, QAM is commonly used as the subcarrier modulation methods.

Different QAM modulation schemes are commonly used, e.g., 4-QAM, 16-QAM, 64-QAM, 256-QAM and so on. Higher order of modulation indicates that the system has the capability to carry higher data rate, in bits per seconds. On the other hand, it also indicates that the system becomes much more sensitive to noise and fading effects. In this thesis, 4-QAM, 16-QAM, and 64-QAM will be used for OFDM uplink transmission.

3.1.2 IDFT

The implementation of orthogonal modulation for *N* subcarriers is achieved by Inverse Discrete Fourier Transform (IDFT) which can be expressed as:

$$x_m(n) = \frac{1}{\sqrt{N}} \sum_{k=0}^{N-1} X_m(k) e^{\frac{2\pi j \cdot kn}{N}} \quad (3\text{-}1)$$

where $x_m(n)$ represents the m^{th} transmitted OFDM symbol sequence and $X_m(k)$ is m^{th} symbol modulated to subcarrier *k*. *N* is length of the IDFT, $n \in [0, N-1]$ is the sample time index, and $k \in [0, N-1]$ is the subcarrier index. The sampling time interval is defined as T_S and then the sampling frequency can be calculated as:

$$F_S = 1/T_S.$$

Thus, the subcarrier spacing can be expressed as:

$$f_S = 1/(N \cdot T_S)$$

The processing of IDFT processing of Equation. (3-1) can be efficiently computed using the Inverse Fast Fourier Transform (IFFT).

3.1.3 Cyclic Prefix

In the presence of multipath propagation, orthogonality is maintained by inserting a guard interval, Δ_g, which is larger than the channel delay spread, which is caused by the frequency selective channel [25]. Otherwise, the received OFDM symbols will suffer from Inter-Symbol Interference (ISI). The Guard Interval (GI) is inserted in time domain, after IFFT operation. It is convenient to use Cycle Prefix (CP), i.e., cyclic extension of the generated OFDM symbol in front of the actual OFDM symbol, because

in this case the orthogonality of subcarriers is maintained. This will increase the time duration for OFDM symbols to:

$$T = N \cdot \mathrm{T}_s + \Delta_g$$

Figure 3-3 shows the process of CP extension.

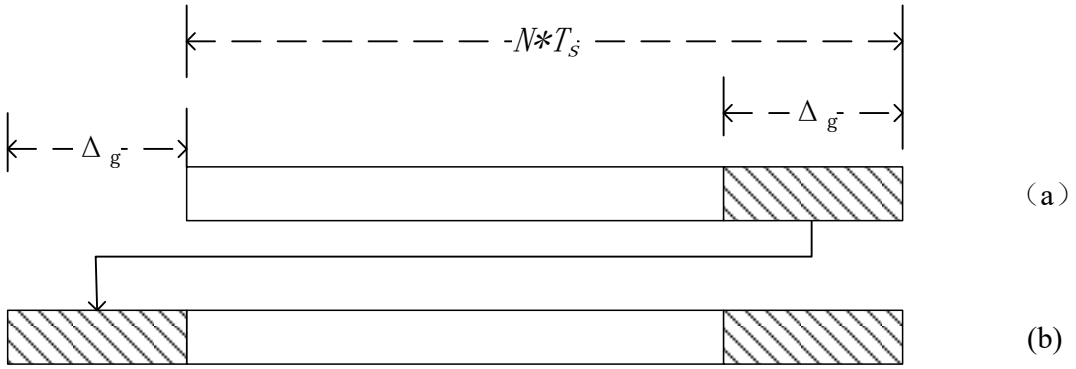

Figure 3-3 *(a) No cyclic prefix, (b) Cyclic prefix inserted*

3.2 Receiver

On the receiver side, a general OFDM system will first translate the serial sequence to parallel sequence according to the length of IFFT and CP, then the cyclic prefix will be removed. After that, the data is fed to Discrete Fourier Transform (DFT) for detecting the subcarrier symbols. In practical implementations, the computationally efficient Fast Fourier Transform (FFT) algorithm is used. The orthogonality is then achieved, which can be shown by expressing the effect of the symbol modulated to subcarrier *k* on the detected symbol in subcarrier *l* as follows [24]:

$$\sum_{l=0}^{N-1} x_m(k) \cdot e^{-\frac{2\pi j \cdot l \cdot n}{N}} = \begin{cases} 1, & l = k \\ 0, & otherwise \end{cases}$$

In order to reconstruct the original information from received data, which is distorted by the channel and additive noise, filtering and channel equalization will be implemented. In this thesis, high-pass filter is employed at the transmitter to avoid the sidelobe effect for the combined NB-IoT signal. Therefore, in the absence of noise, the n^{th} symbol is demodulated by:

$$Y(k) = \sum_{n=0}^{N-1} x_m(k) \cdot e^{-\frac{2\pi j \cdot k \cdot n}{N}}$$

where *Y(k)* is the channel frequency response corresponding to subcarrier *k.*

3.2.1 Frequency Offset

Generally, the uncertainty in carrier frequency is due to a difference of local oscillators in transmitter and receiver that results in a shift in frequency domain. This shift can also be caused by Doppler shift in the channel [26][27]. The carrier frequency offset (CFO) in an OFDM system is the difference between the actual carrier frequency used at the transmitter and the frequency used in the receiver to down-convert the signal to baseband. Each subcarrier experiences a frequency offset which is equal to the CFO.

If the frequency offset is denoted as Δf_c, and $x_m(n)$ and $Y_m(k)$ denote as generated OFDM signal and received signal respectively, then:

$$\Delta k = \frac{\Delta f_c}{f_s}$$

$$Y_m(k) = \sum_{n=0}^{N-1} e^{\frac{2\pi j \cdot (k-\Delta k) \cdot n}{N}} \cdot x_m(n)$$

In general, CFO destroys the orthogonality of subcarriers and introduces ICI. Typically, CFO is required to be less than 1 % of the subcarrier spacing.

3.2.2 Timing Offset

Timing synchronization between transmitter and receiver is essential for OFDM to correctly detect and decode the valid symbols. With the effect of timing offset, phase rotation of subcarriers would be introduced. In general, the cyclic prefix can absorb small timing offsets, but it is required that the joint effect of timing offsets and channel delay spread should be shorter than the CP duration. Precise adjustment of the timing advances of different uplink users is required to achieve this, which requires a rather complicated synchronization process. In case of NB-IoT, the required hand-shaking type synchronization protocol would introduce significant overhead in power

consumption and transmission resource usage, and asynchronous uplink transmission would be greatly preferred.

In this thesis, both frequency offset and timing offset, as well as a nonlinear power amplifier model are introduced to the simulation model in order to examine the effect of windowing and filtering on the related interference leakage issues.

4. SYSTEM DESCRIPTION

This thesis aims to develop effective methods for the enhancement of NB-IoT uplink chain in asynchronous case. Meanwhile, the performance of uplink LTE is also evaluated when one of the resource blocks is shared for asynchronous in-band NB-IoT use. We will concentrate the single-tone NB-IoT transmission case.

4.1 Constant Envelope Modulation

As we mentioned in Chapter 2, OFDM has a very high PAPR that requires a large linear range of power amplifier, which would significantly increase the cost of IoT devices. Otherwise, the nonlinear distortion of the transmitted signal would resulting in performance degradations for both the NB-IoT and the host LTE systems [28]. What's more, operation with a high PAPR in OFDM system is not efficient in terms of energy consumption. Thus, a number of techniques have been developed for reducing the PAPR of OFDM signals. The lowest PAPR (0 dB) at transmitter can be achieved only if the peak power equals to the average power, which means constant envelope modulation.

Time domain windowing methods considered in this thesis will destroy the constant envelope property of single-tone OFDM signals. Also, sub-band filtering, and conventional channel filtering as well, will have the same effect. We will introduce a novel phase rotation scheme which maintains the constant envelop property with root-raised-cosine (RRC) type windowing. Detailed mathematic model to achieve a constant envelope single-tone NB-IoT signal with time-domain windowing will be explained below.

4.2 Symbol Generation model

OFDM signal generation was outlined in Figure 2-2, while our model for single-tone NB-IoT generation is presented in Figure 4-1. Here the core part is the simplest form of OFDM, with one active subcarrier only. Interestingly, in this specific case OFDM is equivalent to SC-FDMA (the OFDM-based single-carrier transmission scheme applied

in the LTE uplink and multi-tone NB-IoT uplink as well). NB-IoT uses so-called π/2-BPSK modulation in the uplink. In our model, a modified phase rotation scheme is adopted to achieve the constant envelop modulation characteristic also in the presence of time-domain windowing.

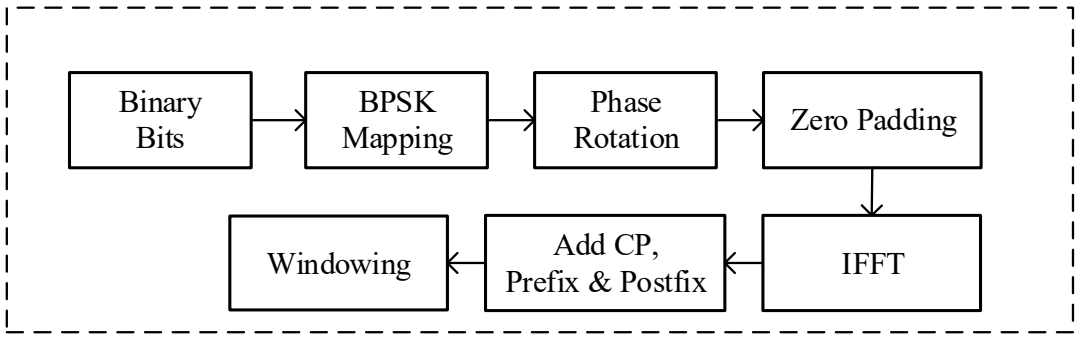

Figure 4-1 *NB-IoT symbol generation*

The symbol generation for NB-IoT signal requires certain phase rotation to overcome the effect of IFFT and time domain windowing to achieve a desirable output. Symbols are generated by:

$$Symbols = 2 \cdot (Bits - 1) \cdot e^{\left(\left(j\cdot\frac{\pi}{2}\right)\cdot([0:N_S-1])\right)} \cdot e^{\left(\frac{2\cdot\pi\cdot k\cdot L_A}{128}\cdot j\right)\cdot([0:N_S-1])} \qquad (4\text{-}1)$$

$$L_A = CP + W$$

where *CP* is the length of cyclic prefix, *W* is the length of the additional cyclic extension for time-domain windowing, and *k* is the subcarrier used single tone NB-IoT. N_s is the length of generated symbols. In Equation. (4-1), the first exponential term corresponds to the phase rotation used for the common π/2-BPSK modulation, while the second exponential term aligns the phases of overlapping cyclic extensions to ±π/2 phase difference.

4.2.1 Zero Padding

In-between OFDM symbols, a guard band is inserted for the duration of the channel. The goal is to make the received symbols mutually independent. That is the reason why the zero-padding is applied. In this thesis, a very special case of NB-IoT is considered where only a single subcarrier is active. Therefore, the input of all the other subcarriers is zero.

$$\boldsymbol{S} = \begin{cases} \begin{bmatrix} x_1(1) & x_2(1) & x_{N_s}(1) \\ 0 & \cdots & 0 \\ \vdots & \ddots & \vdots \\ 0 & \cdots & 0 \end{bmatrix} & k = 0 \\ \begin{bmatrix} 0 & 0 & & 0 \\ \cdots & \cdots & \cdots & \cdots \\ x_2(k) & x_2(k) & & x_{N_s}(k) \\ \vdots & \vdots & \ddots & \vdots \\ 0 & 0 & \cdots & 0 \end{bmatrix} & otherwise \end{cases}$$

4.3 Windowing

In this thesis, windowing refers to time domain-windowing that intends to modify the NB-IoT symbols directly to suppress the sidelobes of its spectrum. The main idea of windowing is to multiply extended NB-IoT symbols in time domain with appropriate windowing configuration that provides the smoothness needed in the transitions between consecutive NB-IoT symbols [29].

There are some restrictions on how to choose the window function. Firstly, the length of transition window has to be equal to the overall extended OFDM symbol duration. What's more, the windowing must not distort the initial data in time domain, including the basic OFDM symbol and the CP extension. As a result, additional cyclic extensions have to be appended as prefix and postfix, as shown in Figure 4-2.

To create the cyclic prefix, $CP+W$ samples are copied from last part of NB-IoT IFFT to its beginning. Besides, the postfix is to add the first W samples to its end. Thus, the time domain symbols are consequently extended from N samples to $N+CP+2\cdot W$ samples. Finally, adjacent symbols are overlapped by W samples in the edge regions [30], which results in a similar result as in CP-OFDM. This process is shown in Figure 4-3

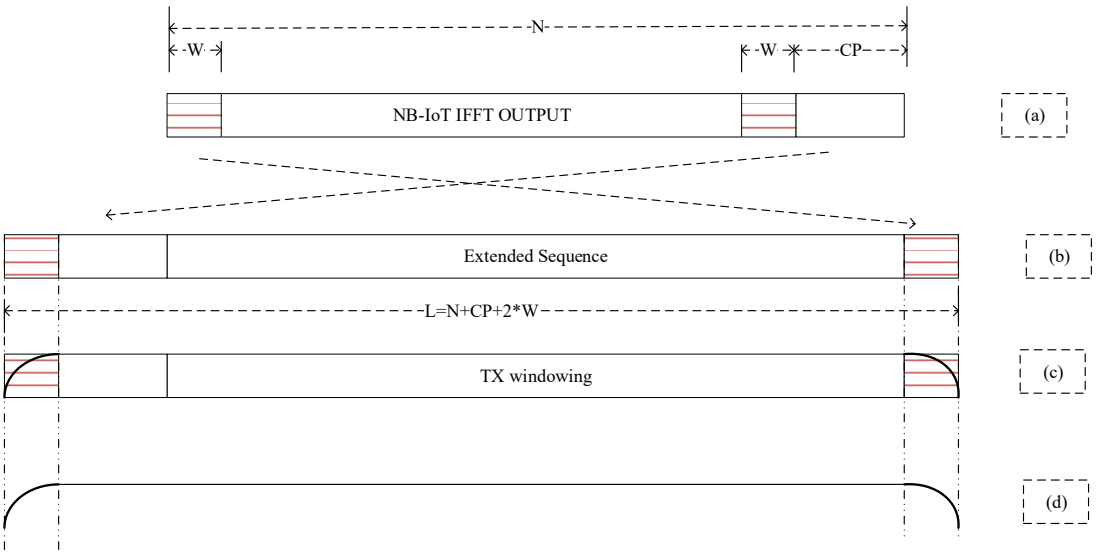

Figure 4-2 *OFDM symbol extension and time-domain windowing (a) IFFT output (b) extended Samples (c) Windowed Samples (d) time domain windowing*

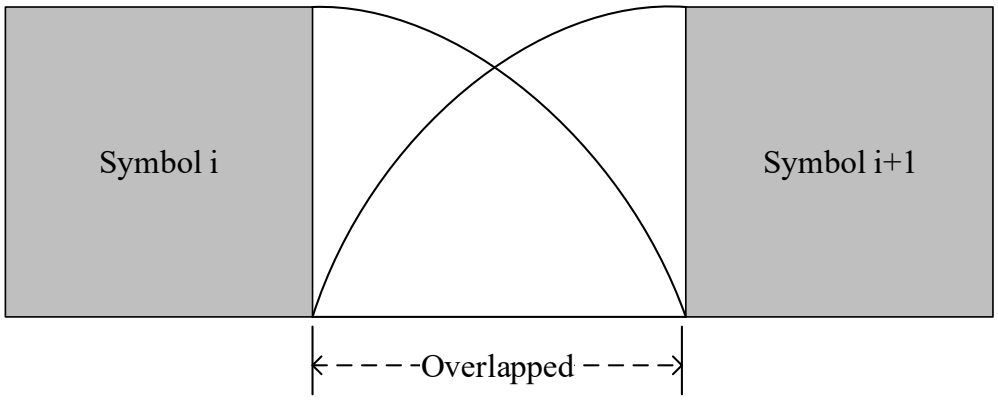

Figure 4-3 *Symbol overlapping*

After the cyclic extension insertion, a window of same length as *N+CP+2*W* is applied. The most common method is to define the transitions of the time domain window as a Raised-Cosine (RC) windows. In this thesis, both Root- Raised-Cosine (RRC) and Raised-Cosine (RC) windowing are considered and compared to evaluate the resulting performance.

A RRC function is defined as:

$$p(i)=\begin{cases}\sqrt{\left(\frac{1}{2}+\frac{\cos\left(\pi+\pi\cdot\frac{i}{W+1}\right)}{2}\right)} & i\le W\\ 1 & i>W\ \&\ i\le(L-W)\\ \sqrt{\left(\frac{1}{2}+\frac{\cos\left(\pi\cdot\frac{i+W-L}{W+1}\right)}{2}\right)} & i>(L-W)\end{cases}$$

where L is the length of the time-window, and W is length of both transition parts.

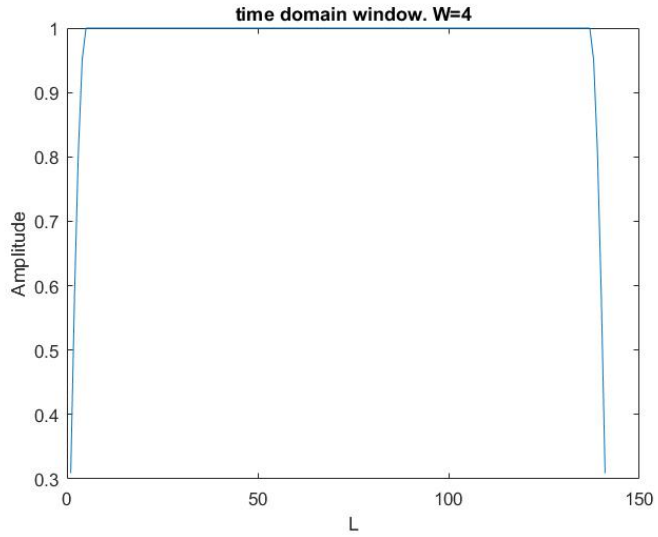

Figure 4-4 *RRC-type time-domain of windowing function with L=141 and W=4.*

According to the equations and Figure 4-4 above, it can be seen that the RRC window is symmetrical, i.e.:

$$p(1)=p(L),p(2)=p(L-1),\cdots,p(W)=p(L-W+1) \tag{4-2}$$

$$p(1)^2+p(W)^2=\ p(2)+p(W-1)^2=,\cdots,=1 \tag{4-3}$$

As for the RC function, it is very similar with RRC windowing, and its generation model can be expressed as:

$$p(i) = \begin{cases} (\frac{1}{2} + \frac{\cos(pi + pi \cdot \frac{i}{W+1})}{2} & i \leq W \\ 1 & i > W \;\&\; i \leq (L - W) \\ \frac{1}{2} + \frac{\cos(pi \cdot \frac{i + W - L}{W+1})}{2} & i > (L - W) \end{cases}$$

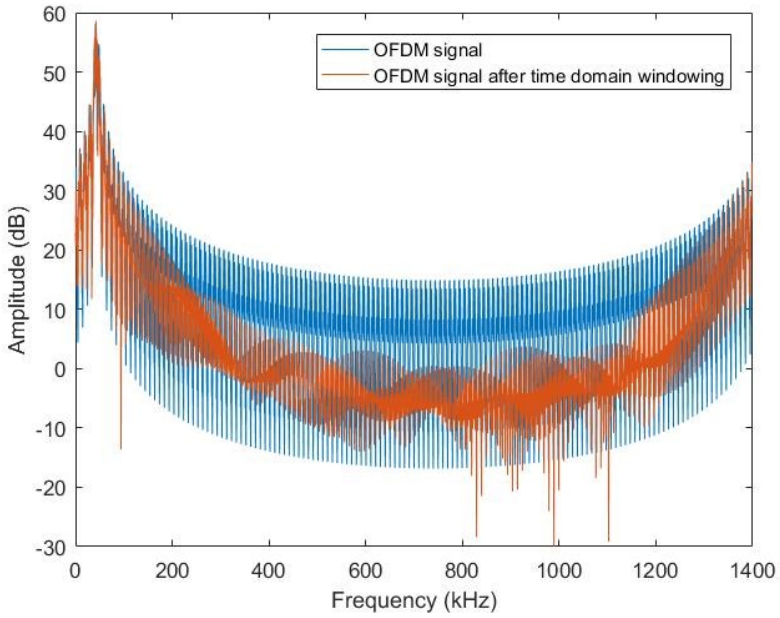

Figure 4-5 *Effect of RRC time-domain windowing on NB-IoT single-tone signal with CP=5, W=4*

The suppression performance of windowing function is depicted in Figure 4-5. The frequency spectrum of NB-IoT signal shows a relatively high suppression performance compared to the basic CP-OFDM. The useful band remains the same as before, but the sidelobes are greatly decreased.

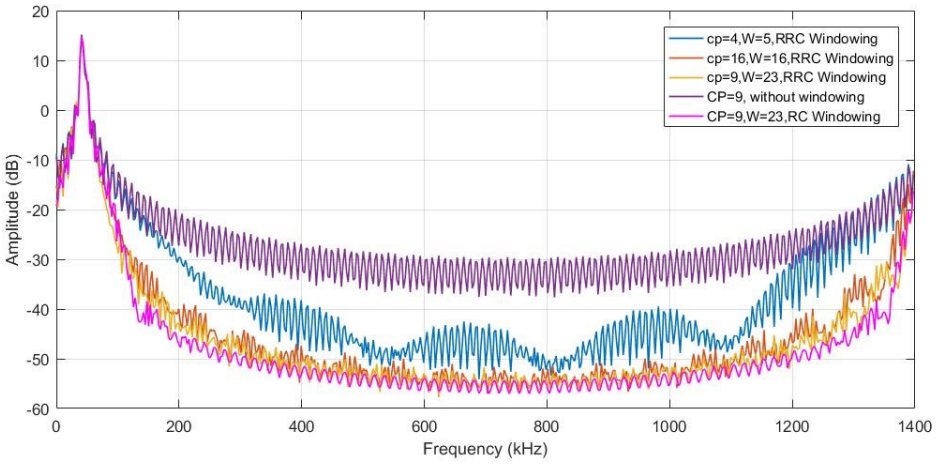

Figure 4-6 *Effect of RC and RRC windowing with different CP& window lengths.*

What's more, the performance of time-domain windowing depends greatly on the lengths of the prefix and postfix extension parts, i.e., the length of the window transition intervals. Figure 4-6 shows the NB-IoT spectra with different CP and window extension lengths for the overall extension lengths of 9 and 32 samples. The longer the transition interval is, the better the performance regarding the out-of-band spectrum suppression. Obviously, it can also be concluded that windowing work well on sidelobe suppression when compared to non-windowing cases but with same CP length.

Generally, for a given overall symbol duration, the effective CP length has to be reduced when time-domain windowing is applied. While the CP length is a fixed parameter in existing OFDM standards, its partitioning to the effective CP part and windowing overlap part may be possible for specific application scenarios. In the case studies of this thesis, we consider the 1.4 MHz LTE system with 128 subcarriers. Here the normal CP-length is 10 samples for the first OFDM symbols of each slot (consisting of 7 OFDM symbols) and 9 samples for the other OFDM symbols. However, there is an option to use extended CP length, with 6 OFDM symbols per slot and CP length of 32. The results of Figure 4-6 indicate clearly that there are much better possibilities to control the NB-IoT spectrum using time-domain windowing in the extended CP case.

4.4 Inverse Fourier Transform

The IFFT transform is defined as:

$$Y(k) = \sum_{l=0}^{N-1} x_m(k) \cdot W_N^{-kn}$$

where W_n is defined as:

$$W_N = e^{\left(\frac{-2\pi j}{N}\right)}$$

The IFFT matrix is defined by the elements W_n^{-n*k} as follows:

$$\mathbf{W} = \frac{1}{N}\begin{bmatrix} W_n^{-0\cdot 0} & W_n^{-0\cdot 1} & \cdots & W_n^{-0\cdot(N-1)} \\ W_n^{-1\cdot 0} & W_n^{-1\cdot 1} & & W_n^{-1\cdot(N-1)} \\ \vdots & \vdots & \ddots & \vdots \\ W_n^{-(N-1)\cdot 0} & W_n^{-(N-1)\cdot 1} & \cdots & W_n^{-(N-1)\cdot(n-1)} \end{bmatrix}$$

$$= \frac{1}{N}\begin{bmatrix} 1 & 1 & \cdots & 1 \\ 1 & e^{\left(\frac{2\pi j\cdot 1}{N}\right)} & & e^{\left(\frac{2\pi j\cdot(N-1)}{N}\right)} \\ 1 & e^{\left(\frac{2\pi j\cdot 2}{N}\right)} & \ddots & e^{\left(\frac{2\pi j\cdot(N-1)\cdot 2}{N}\right)} \\ \vdots & \vdots & & \vdots \\ 1 & e^{\left(\frac{2\pi j\cdot(N-1)}{N}\right)} & \cdots & e^{\left(\frac{2\pi j\cdot(N-1)\cdot(N-1)}{N}\right)} \end{bmatrix}$$

4.5 Single-tone NB-IoT signal generation model

There are two cases which deserved to be discussed in the single-tone NB-IoT context. *(i)* The Direct Current (DC) subcarrier (k=0) is applied or *(ii)* more general cases where $k \neq 0$.

As mentioned above, NB-IoT symbols are generated as:

$$Symbols = 2 \cdot (Bits - 1) \cdot e^{\left((j\cdot\frac{\pi}{2})\cdot([0:Ns])\right)} \cdot e^{\left(\frac{2\cdot\pi\cdot k\cdot(CP+W)}{128}\cdot j\right)\cdot([0:Ns])}$$

where

$$2 \cdot (Bits - 1) \in \{1, -1\}$$

If k=0, the latter complex exponential term is unity, and the scheme is equivalent to the basic π/2-BPSK, without any additional phase rotation. More details are explained later in this section.

The π/2-BPSK scheme introduces 90 degrees phase-shifting between consecutive symbols, resulting in the following symbol sequence:

$$e^{\left(\left(j\cdot\frac{pi}{2}\right)*[0:13]\right)} = [1, j, -1, -j, 1, j, -1, -j, 1, j, -1, -j, 1, j],$$

The output of IFFT is obtained as follows:

$\boldsymbol{x} = IFFT(\boldsymbol{S})$=

$$\frac{1}{N}\begin{bmatrix} 1 & 1 & \cdots & 1 \\ 1 & e^{\left(\frac{2\pi j\cdot 1}{N}\right)} & & e^{\left(\frac{2\pi j\cdot(N-1)}{N}\right)} \\ 1 & e^{\left(\frac{2\pi j\cdot 2}{N}\right)} & \ddots & e^{\left(\frac{2\pi j\cdot(N-1)\cdot 2}{N}\right)} \\ \vdots & \vdots & & \vdots \\ 1 & e^{\left(\frac{2\pi j\cdot(N-1)}{N}\right)} & \cdots & e^{\left(\frac{2\pi j\cdot(N-1)\cdot(N-1)}{N}\right)} \end{bmatrix}$$

$$\cdot\begin{bmatrix} x_1(1) & x_2(1) & x_{N_s}(1) \\ 0 & \cdots & 0 \\ \vdots & \ddots & \vdots \\ 0 & \cdots & 0 \end{bmatrix} = \frac{1}{N}\begin{bmatrix} x_1(1) & x_2(1) & \cdots & x_{N_s}(1) \\ x_1(1) & x_2(1) & & x_{N_s}(1) \\ & \vdots & \ddots & \vdots \\ x_1(1) & x_2(1) & \cdots & x_{N_s}(1) \end{bmatrix}$$

Multiplied with RRC windowing function and implement overlapping, we obtain:

$$z_2(1) = x_1(1)\cdot p(L-W+1) + x_2(1)\cdot p(1)\cdot j$$

$$z_2(2) = x_1(1)\cdot p(L-W+2) + x_2(1)\cdot p(2)\cdot j$$

$$\vdots$$

$$z_w(2) = x_1(1)\cdot p(L) + x_2(1)\cdot p(W)\cdot j$$

According to the property of RRC windowing expressed in Equation.(4-2) and Equation.(4-3) Follows that:

$$z_2(1) = x_1(1)\cdot p(W) + x_2(1)\cdot p(1)\cdot j$$

$$z_2(2) = x_1(1)\cdot p(W-1) + x_2(1)\cdot p(2)\cdot j$$

$$\vdots$$

$$z_w(2) = x_1(1)\cdot p(L) + x_2(1)\cdot p(W)\cdot j$$

$$|z_2(1)| = \sqrt{x_1(1)^2 \cdot p(W)^2 + (x_2(1)^2 \cdot p(1)^2}$$

For the single-tone binary modulation:

$$x_1(1)^2 = x_2(1)^2$$

Therefore, according to Equation. (4-3):

$$|z_2(1)| = |x_1(1)| = |x_2(1)|$$

This operation can be done for the whole matrix calculation, which manifests that the output signal has constant envelope. The general idea can also be explained as in Figure 4-7.

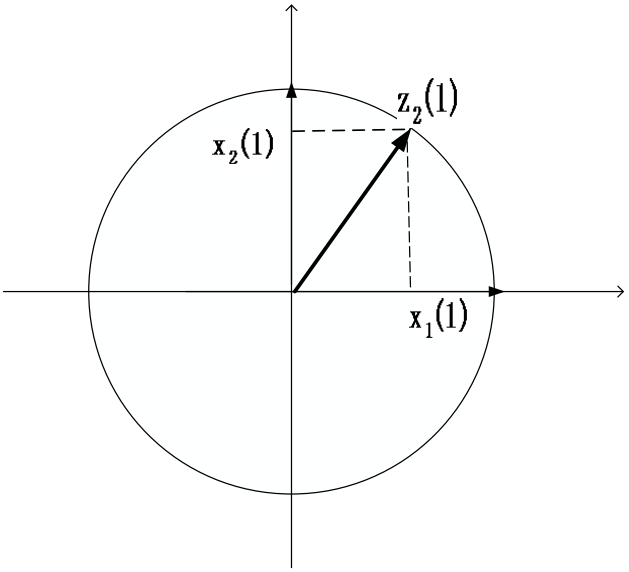

$$p(1)^2 + p(w)^2 = 1$$
$$z_2(1) = x_1(1) \cdot p(1) + x_2(1) \cdot p(w)$$
$$|z_2(1)| = \sqrt{(x_1(1) \cdot p(1))^2 + (x_2(1) \cdot p(w))^2} =$$
$$\sqrt{x_1(1)^2 \cdot p(1)^2 + x_2(1)^2 \cdot p(w)^2} = |x_1(1)| = |x_2(1)|$$

Figure 4-7 *Polar coordinate based analysis of window overlap*

Here *p(1)* and *p(w)* represent the weighting factors. Vectors $x_1(1)$ and $x_2(1)$ represent complex overlapping symbol, and $z_2(1)$is an output sample.

As for more general case with $k \neq 0$,

$$\boldsymbol{S} = \begin{bmatrix} 0 & 0 & & 0 \\ \cdots & \cdots & \cdots & \cdots \\ x_1(k) & x_2(k) & & x_{N_s}(k) \\ \vdots & \vdots & \ddots & \vdots \\ 0 & 0 & \cdots & 0 \end{bmatrix}$$

$$\boldsymbol{x} = IFFT(\boldsymbol{S})$$

$$= \frac{1}{N} \begin{bmatrix} W_n^{-0\cdot 0} & W_n^{-0\cdot 1} & \cdots & W_n^{-0\cdot(N-1)} \\ W_n^{-1\cdot 0} & W_n^{-1\cdot 1} & & W_n^{-1\cdot(N-1)} \\ \vdots & \vdots & \ddots & \vdots \\ W_n^{-(N-1)\cdot 0} & W_n^{-(N-1)\cdot 1} & \cdots & W_n^{-(N-1)\cdot(n-1)} \end{bmatrix} \begin{bmatrix} 0 & 0 & & 0 \\ \cdots & \cdots & \cdots & \cdots \\ x_1(k) & x_2(k) & & x_{N_s}(k) \\ \vdots & \vdots & \ddots & \vdots \\ 0 & 0 & \cdots & 0 \end{bmatrix}$$

$$= \frac{1}{N} \begin{bmatrix} x_1(k) & x_2(k) & \cdots & sym_s \\ W_n^{-1\cdot k} \cdot x_1(k) & W_n^{-1\cdot k} \cdot x_2(k) & & W_n^{-1\cdot k} \cdot x_{N_s}(k) \\ \vdots & & \ddots & \vdots \\ W_n^{-(N-1)\cdot k} \cdot x_1(k) & W_n^{-(N-1)\cdot k} \cdot x_2(k) & \cdots & W_n^{-(N-1)\cdot k} \cdot x_{N_s}(k)_s \end{bmatrix}$$

$$= \frac{1}{N} \begin{bmatrix} x_1(k) & x_2(k) & \cdots & x_{N_s}(k) \\ e^{(\frac{2\pi j\cdot k}{N})} \cdot x_1(k) & e^{(\frac{2\pi j\cdot k}{N})} \cdot x_2(k) & & e^{(\frac{2\pi j\cdot k}{N})} \cdot x_{N_s}(k) \\ \vdots & & \ddots & \vdots \\ e^{(\frac{2\pi j\cdot(N-1)\cdot k}{N})} \cdot x_1(k) & e^{(\frac{2\pi j\cdot(N-1)\cdot k}{N})} \cdot x_2(k) & \cdots & e^{(\frac{2\pi j\cdot(N-1)\cdot k}{N})} \cdot x_{N_s}(k) \end{bmatrix}$$

If we take CP and overlap extension into consideration, the output matrix can be expressed as:

$$\boldsymbol{Z} = \frac{1}{N} \begin{bmatrix} e^{(\frac{2\pi j\cdot(N-CP-W)\cdot k}{N})} \cdot x_1(k) & e^{(\frac{2\pi j\cdot(N-CP-W)\cdot k}{N})} \cdot x_2(k) & & e^{(\frac{2\pi j\cdot(N-CP-W)\cdot k}{N})} \cdot x_{N_s}(k) \\ e^{(\frac{2\pi j\cdot(N-CP-W+1)\cdot k}{N})} \cdot x_1(k) & e^{(\frac{2\pi j\cdot(N-CP-W+1)\cdot k}{N})} \cdot x_2(k) & \cdots & e^{(\frac{2\pi j\cdot(N-CP-W+1)\cdot k}{N})} \cdot x_{N_s}(k) \\ \vdots & \vdots & & \vdots \\ x_1(k) & x_2(k) & & x_{N_s}(k) \\ e^{(\frac{2\pi j\cdot k}{N})} \cdot x_1(k) & e^{(\frac{2\pi j\cdot k}{N})} \cdot x_2(k) & & e^{(\frac{2\pi j\cdot k}{N})} \cdot x_{N_s}(k) \\ \vdots & & \ddots & \vdots \\ e^{(\frac{2\pi j\cdot(N-1)\cdot k}{N})} \cdot x_1(k) & e^{(\frac{2\pi j\cdot(N-1)\cdot k}{N})} \cdot x_2(k) & & e^{(\frac{2\pi j\cdot(N-1)\cdot k}{N})} \cdot x_{N_s}(k) \\ x_1(k) & x_2(k) & \cdots & x_{N_s}(k) \\ \vdots & \vdots & & \vdots \\ e^{(\frac{2\pi j\cdot(W-1)\cdot k}{N})} \cdot x_1(k) & e^{(\frac{2\pi j\cdot(W-1)\cdot k}{N})} \cdot x_2(k) & & e^{(\frac{2\pi j\cdot(W-1)\cdot k}{N})} \cdot x_{N_s}(k) \end{bmatrix}$$

The edge of sym_i is overlapped with adjacent symbols sym_{i+1}. This operation is summarized in Table 1.

Table 1: *Windowed symbol overlapping model*

Postfix of symbol (i)	Prefix of symbol (i+1)
$x_i(k)$	$e^{(\frac{2\pi j\cdot(N-CP-W)\cdot k}{N})}\cdot x_{i+1}(k)$
$e^{(\frac{2\pi j\cdot k}{N})}\cdot x_i(k)$	$e^{(\frac{2\pi j\cdot(N-CP-W+1)\cdot k}{N})}\cdot x_{i+1}(k)$
⋮	⋮
$e^{(\frac{2\pi j\cdot(W-1)\cdot k}{N})}\cdot x_i(k)$	$e^{(\frac{2\pi j\cdot(N-CP+1)\cdot k}{N})}\cdot x_{i+1}(k)$

Polar coordinates are then utilized to better explain the idea of constant envelope procedure in Figure 4-8.

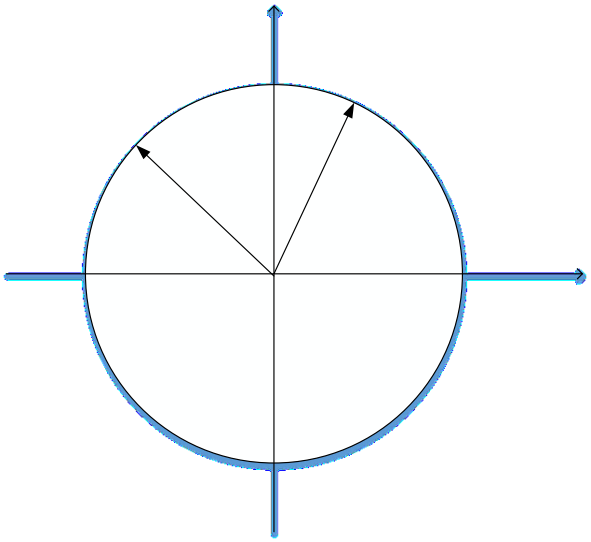

$$x_i(k) = a + b\cdot j$$
$$x_{i+1}(k) = c + d\cdot j$$
$$z_i(k) = x_i(k)\cdot p(l) + x_{i+1}(k)\cdot p(w)$$

Figure 4-8 *Polar coordinate based analysis of window overlap in general case*

Same as before, $z_i(k)$ is the output symbol and $x_i(k)$ and $x_{i+1}(k)$ are two overlapped symbols, *a,b,c,d* are corresponding real/imaginary parts.

The output symbol can be expressed as follows:

$$|z_i(k)| = |a \cdot p(1) + b \cdot p(1) \cdot j + c \cdot p(1) + d \cdot p(1) \cdot j|$$

$$= |(a \cdot p(1) + c \cdot p(w)) + (b \cdot p(1) + d \cdot p(w)) \cdot j|$$

$$= \sqrt{(a \cdot p(1) + c \cdot p(w))^2 + (b \cdot p(1) + d \cdot p(w))^2}$$

$$= \sqrt{(a^2 + b^2) \cdot p(1)^2 + (c^2 + d^2) \cdot p(w)^2 + (ac + bd) \cdot 2 \cdot p(1) \cdot p(w)}$$

$\sqrt{(ac + bd) \cdot 2 \cdot p(1) \cdot p(w)}$ equals to zero only when $\frac{pi}{2}$ phase rotation for previous inner adjacent subcarriers is employed.

What's more, phase compensation θ also should be introduced according to the subcarriers that NB-IoT occupied.

$$\theta = e^{(\frac{2\pi \mathbf{j} \cdot (N - CP - W) \cdot k}{N})}$$

4.6 Filtering

In practice, NB-IoT sequences and OFDM sequences are transmitted together through the same carriers. This means that data from different user equipment will summed totally regardless different power strengths. In order to decrease interference from different kinds of users, filtering is then implemented. In general, filtering reduces the out-of-band radiation, which would cause interference to the users of adjacent resource blocks, or decrease the spectral efficiency if wider guard bands are used. The disadvantages of filtering is also apparent: it can cause some increase in the peak transmission power, and it introduces some amount of in-band distortion that results in error-rate degradation.

In this thesis, filtering is applied on both NB-IoT and OFDM signals. The passband of filtering is related to the center frequency of corresponding active subcarriers. Without loss of generality, we utilize a simplified system model, where the NB-IoT is centered at DC. Then a lowpass filter is applied with NB-IoT and high-pass filter is designed for OFDM signals. The main purpose is to reduce the out-of-band radiation as much as

possible to ensure that the sidelobes of both signals will not interference with each other. The time and frequency responses both filters used in the simulations of this thesis are shown in Figure 4-9and Figure 4-10.

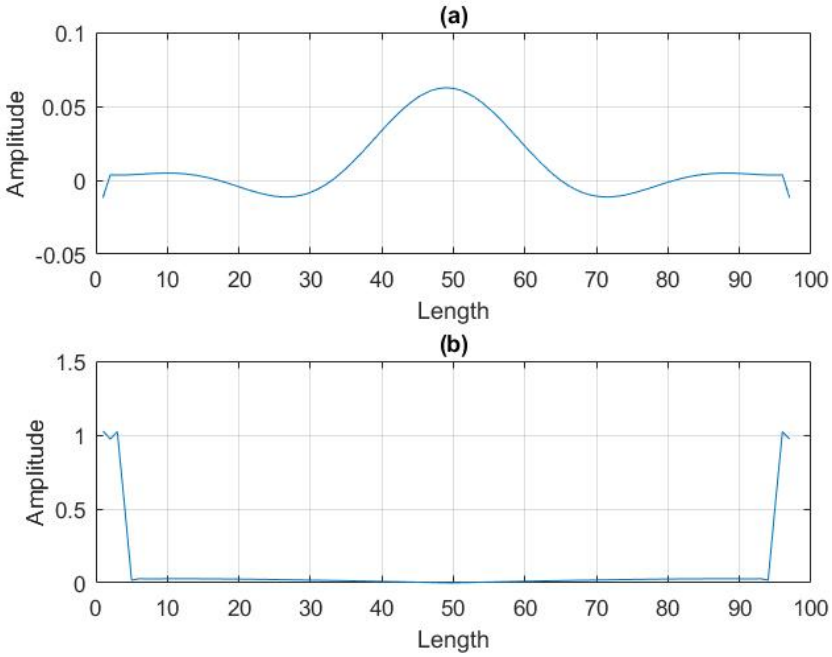

Figure 4-9 *Low-pass filter in time & frequency domain for NB-IoT*

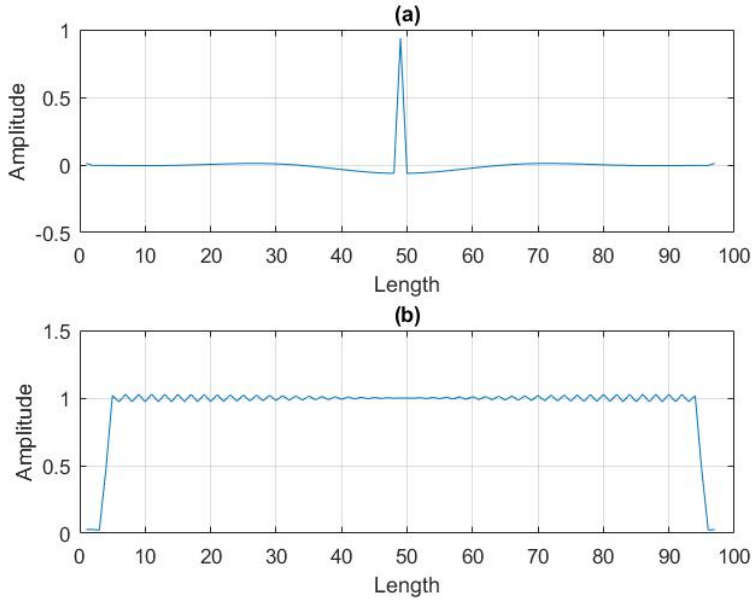

Figure 4-10 *High-pass filter in time & frequency domain for LTE*

4.6.1 Matched Filters

Matched filters refer to the optimum filters that are usually applied at the receiver to enhance the link performance. In general, the received signal consists of a transmitted signal that is distorted by by channel. The channel noise is usually considered as additive Gaussian white noise. To minimize the noise effect, this requires a matched filter. In one-words, matched filters maximize the SNR when the channel impulse response is known and the received signal is affected by additive white Gaussian noise. However, in a filtered OFDM system, the main purpose of the receiver sub-band filtering is to suppress interference leakage from the active subcarriers of adjacent, possibly asynchronous, resource blocks. The filtering requirements are similar to those of the transmitter side, so it is natural to use the same filters on both sides. Since linear-phase FIR filters are used, this is also a matched filter solution.

The representation of matched filter is shown in Figure 4-11.

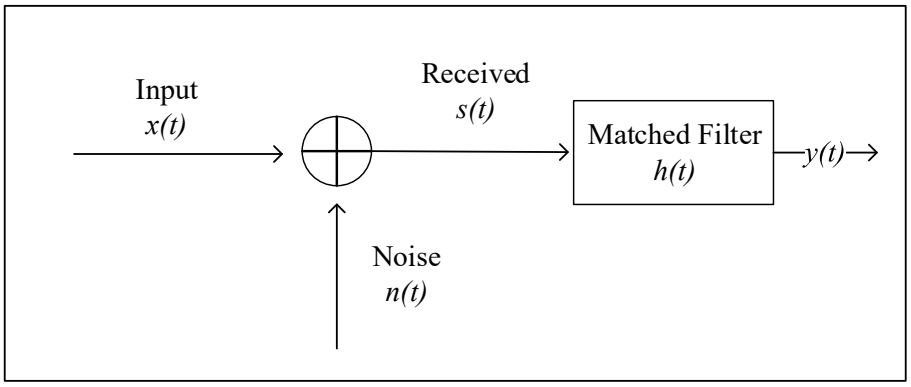

Figure 4-11 *Matched filter in receiver*

For a received signal *s(t)*, transmitted signal *x(t)* and noise *n(t)*.

$$s(t) = x(t) + n(t)$$

$$y(t) = s(t) * h(t) = x(t) * h(t) + n(t) * h(t)$$

Considering there is filtering implemented at transmitter, the simplest matched filter h(t) or equivalently frequency response *H(w)* are corresponding to the filter at the transmitter.

The effects of filtering on the NB-IoT and LTE signals are evaluated through simulation in Chapter 5. The testing model for NB-IoT is shown in Figure 4-12. In this thesis, the matched filters are same as the transmit filters. The main purpose of matched filter is to eliminate out-of-band interference and ensure the transmission quality.

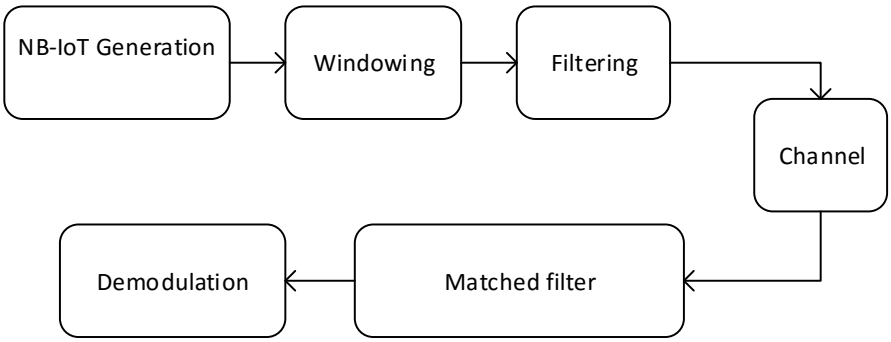

Figure 4-12 *Testing system to evaluate the link performance of filtered NB-IoT.*

4.7 Power Amplifier

Power Amplifier (PA) is a device that amplifies the signal to the targeted transmission power level. Ideally, a power amplifier increases the signal strength linearly according to its gain, while in practice power amplifiers saturate at some point because of electronic circuit limitations and the used supply voltage. This range of limitation is named as nonlinear part of power amplifier [31][32]. Therefore, if a signal with high PAPR passes through a power amplifier, there is huge probability of causing nonlinear distortion. This results in clipping or distortion of the output signal. The clipping of a signal in frequency domain can be considered as increased sidelobes of original signal, which can cause interference to the adjacent subcarriers.

The ideal situation would be a PA operating within the linear range, close to saturation point, so that the signal power is well increased while less distortion is introduced. The various regions of operation of a power amplifier are shown in Figure 4-13.

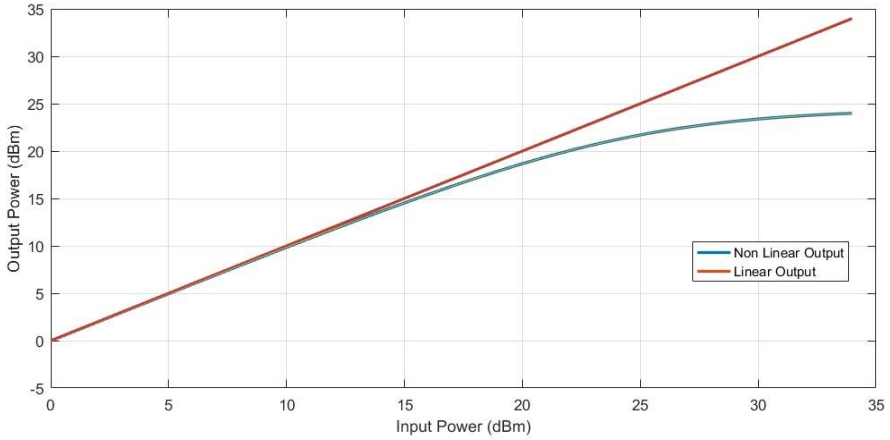

Figure 4-13 *Response of a nonlinear power amplifier model*

In this simulation, a PA model with nonlinear AM-AM (Amplitude modulation-Amplitude modulation) conversion characteristic is employed. In the AM-AM power amplifier model [33], the nonlinear distortion will only effect on the amplitude, but its phase is not affected.

4.7.1 RAPP MODEL

The Rapp model is defined as[34]:

$$S_{out} = \frac{S_{in}}{((1 + \frac{|S_{in}|}{S_{sat}})^{2 \cdot p})^{\frac{1}{2 \cdot p}}}$$

where S_{in} and S_{out} are the PA input signal and output signal, respectively. S_{sat} is the saturation level parameter of PA and p is 'smooth factor' that controls the smoothness of the transition from linear region to saturation region, typically p is in the order of 2.5. The Rapp model is usually considered as a realistic model for semiconductor power amplifiers operating with relatively narrow bandwidth, like the 1.4 MHz LTE case.

4.7.2 Effect of Nonlinear Distortion on Constellation

The effect of nonlinear distortion due to PA appears usually as clipping of the signal in time-domain and it can also be seen as compression of the symbol constellation. Figure

4-14 and Figure 4-15 represent the constellation diagrams for BPSK modulation signals subject to the Rapp model of nonlinearity with two different Back-Offs (BO) and also that of the linear PA model. It may be noticed from the figures that the effect of nonlinearity on BPSK constellation can be seen as compression. Still all the points of the constellation are affected rather linearly. In other words, because of simple modulation of BPSK, the decision regions of the constellation points do not change. In this model, the output power level is significantly reduced with very small back-off. This effect is compensated in the performance simulations such that the transmission power level is always the same while the back-off is varied.

A power amplifier can be operated with high input back-off in the linear region but at the expense of efficiency. In other words, lower back-off gives higher efficiency but it distorts the signal. In practice, a tradeoff has to be found between the power efficiency and acceptable level of nonlinear distortion.

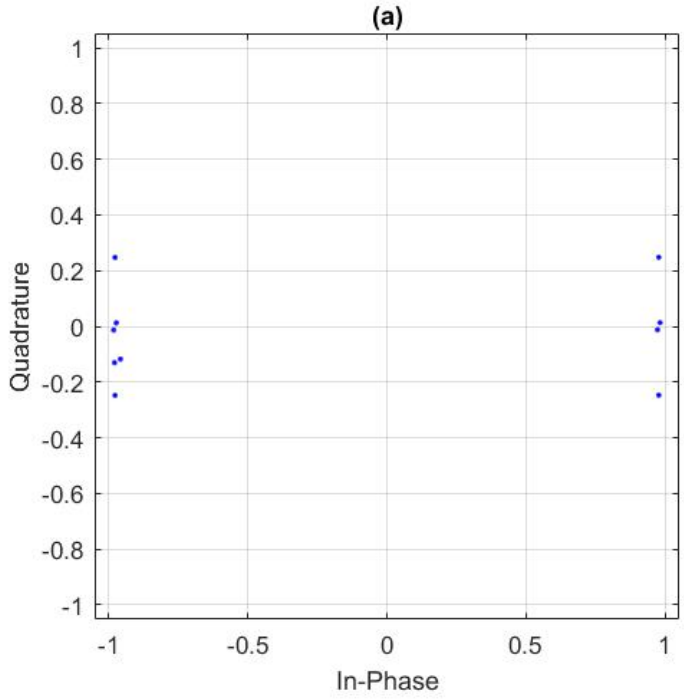

Figure 4-14 *Before Power Amplifier, CP=5,W=4*

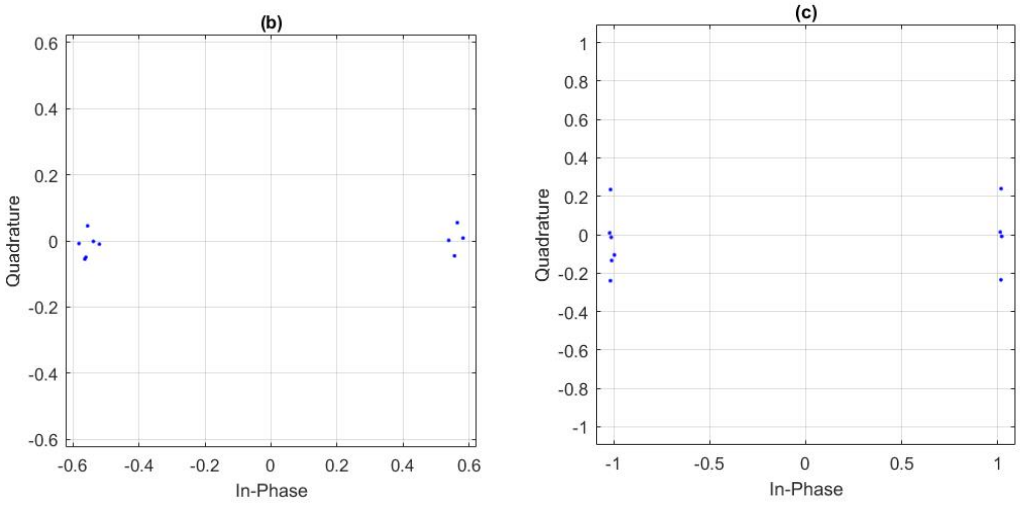

Figure 4-15 *After Power Amplifier (b) Back-off= -6 dB (c) Back-off=6 dB*

4.7.3 Effect of Nonlinear Distortion in Power Spectrum

Power spectrum is the distribution of the power of the signal as a function of frequency. For a single-tone transmission, the appearance of nonlinear distortion is easy to analyze. Figure 4-16 shows the spectra with three different back-off values (the 'Before PA' – plot corresponds to very high back-off). We can see significant spectral regrowth with small back-off. Figure 4-17 shows the spectra with different windowing schemes when the back-off is -6 dB. Longer window transition gives clearly lower spectral regrowth. Also, a slight benefit can be seen for the RRC windowing scheme which maintains the constant envelope of the π/2-BPSK signal.

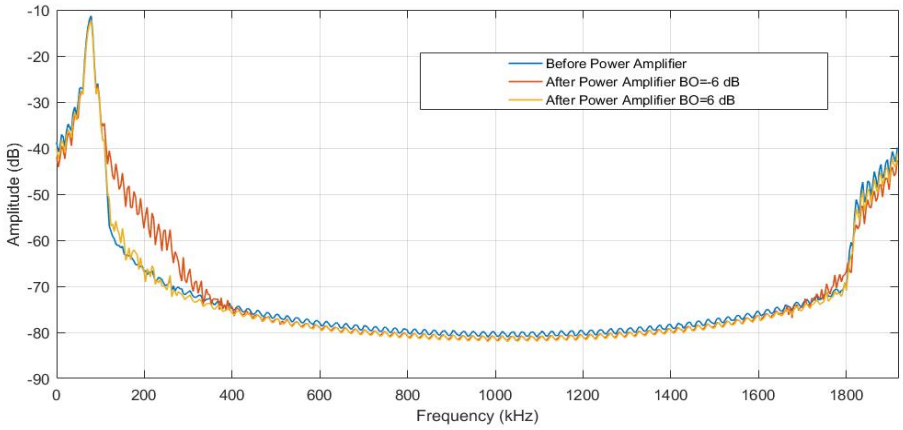

Figure 4-16 *Comparison of signal before PA and after PA (Back-off=-6/6 dB), CP=5, W=4*

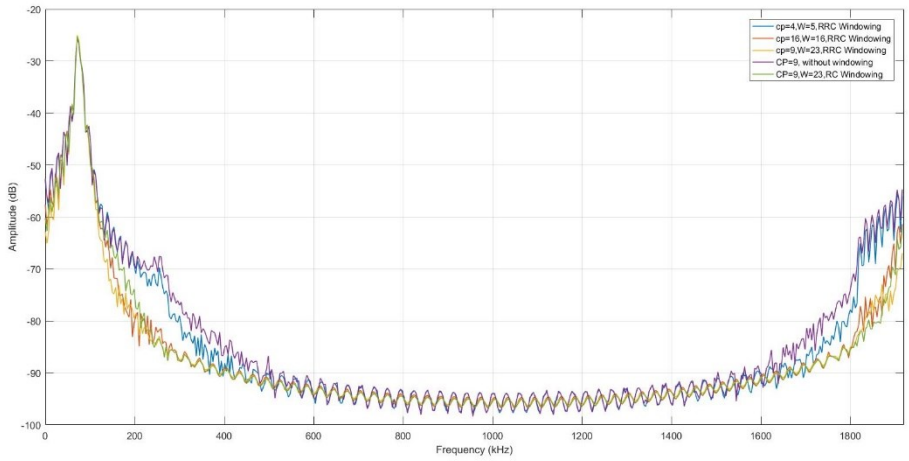

Figure 4-17 *Comparison of different Windowed Signal after PA with -6 dB back-off*

5. PERFORMANCE ANALYSIS OF PROPOSED SYSTEM

In this section, frequency offset (CFO) and timing offset (TOF) are both introduced in OFDM signals. The effect of asynchronous NB-IoT uplink operation will be studied considering realistic scenarios regarding the power level differences between NB-IoT and LTE signals.

5.1 Performance analysis of NB-IoT Link

5.1.1 NB-IoT Performance Analysis Model

The NB-IoT communication systems are inherited from existing LTE systems and they are here assumed to occupy one resource block in uplink transmissions. The system model used in simulations is shown in Figure 5-1.

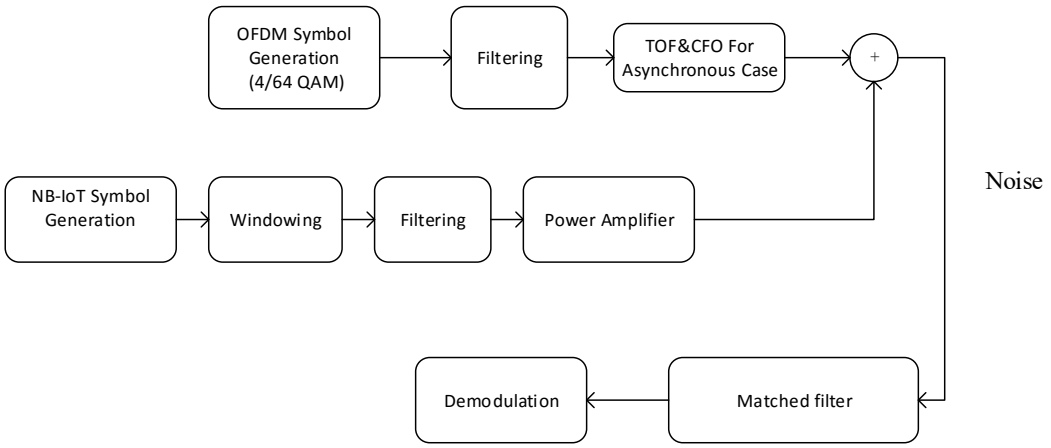

Figure 5-1 *Asynchronous NB-IoT Uplink model*

The worst-case timing offset corresponding to half of the OFDM symbol duration (0.03125 ms), and worst-case frequency offset of half subcarrier spacing (7.5 kHz) are introduced to the LTE signal, assuming that the receiver is synchronized to the NB-IoT transmission. Both the frequency offset and timing offset are implemented which would

lead to asynchronous signals at the base-station receiver are simulated. Additive White Gaussian Noise (AWGN) is then generated and added to the received signal.

5.1.2 LTE Performance Analysis Model

Here the system model is presented from the LTE receiver's point of view. Now the timing and frequency offset is introduced to the NB-IoT link, as shown in Figure 5-2. Again, both the frequency offset and timing offset that lead to asynchronous signals at the base-station receiver are introduced during the transmission. The effect of asynchronous NB-IoT will then introduce additional interference to LTE signal affecting its error-rate performance.

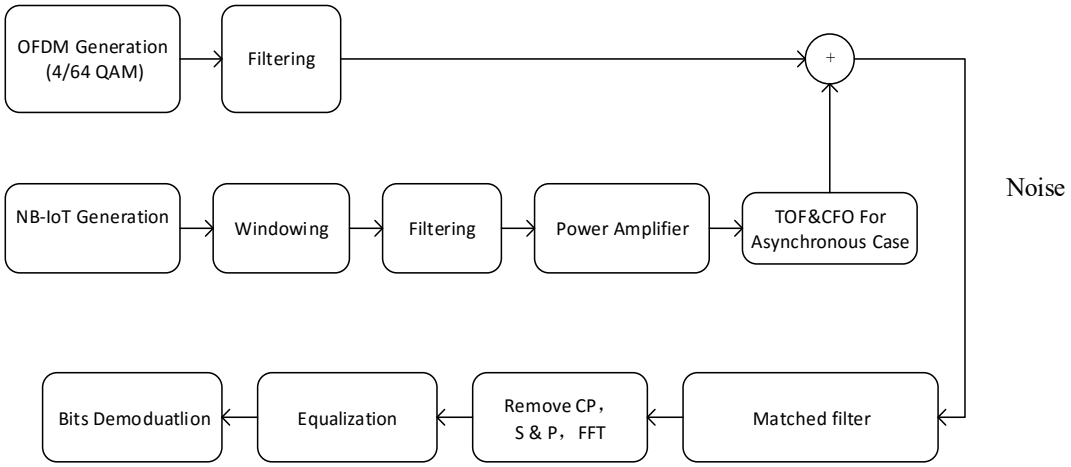

Figure 5-2 *Asynchronous in LTE Uplink channel*

At the receiving end of this model, the signal is first passed through a matched filter which is designed to eliminate the out-of-band interferences and noise. The passband of the matched filter corresponding to the LTE signal, suppressing the interference from NB-IoT but at same time, causes negligible additional distortion on the signal itself.

5.1.3 Simulated System Configuration

Generally, one time-slot of LTE system equals to 0.5 ms. The number of OFDM symbols contained in each time slot is dependent on the CP mode: *(i)* normal CP mode in which each slot has 7 symbols or *(ii)* extended CP mode with 6 symbols in one slot. The spacing between subcarriers is 15 kHz. The model is designed based on the 1.4

MHz LTE system. It is implemented with 128-point IFFT; hence the CP length is defined as CP=9 or CP=32 in normal cases and extended cases respectively. The sampling frequency is 1.92 Mhz. The useful band consists of 6 resource blocks (RB) and each RB contains 12 subcarriers. Therefore, the number of active subcarriers is 72 that occupies about 1.2MHz of spectrum. There is one RB is reserved for NB-IoT among these 6 useful RBs and the actual number of active subcarrier for LTE is 60. Consequently, the transmission of NB-IoT will not affect the carrier bandwidth and there remains 100 kHz as guard-bands on both sides.

Table 2 *Simulated system configuration*

Parameters	Values
Active LTE subcarriers	60
Active NB-IoT subcarriers	1
IFFT size	128
LTE Modulation Methods	4QAM/64QAM
NB-IoT modulation Methods	π/2-BPSK
Sampling Frequency	1.92 MHz
Subcarrier spacing	15 kHz
Filter Order	97
P (RAPP model)	2.5.

5.1.4 Effect of Filtering

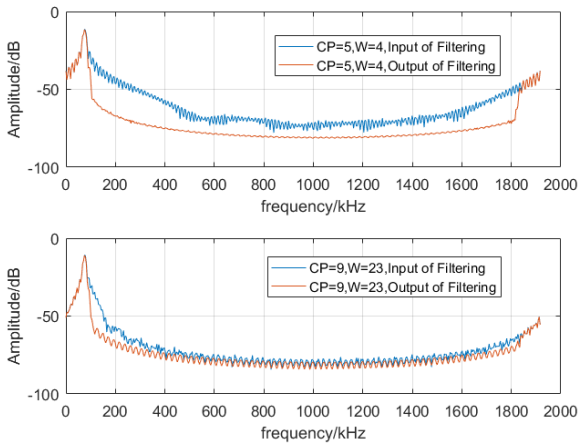

Figure 5-3 *Effect of different filtering windowing configurations. (a) CP=4, W=5 (b) CP=9, W=23*

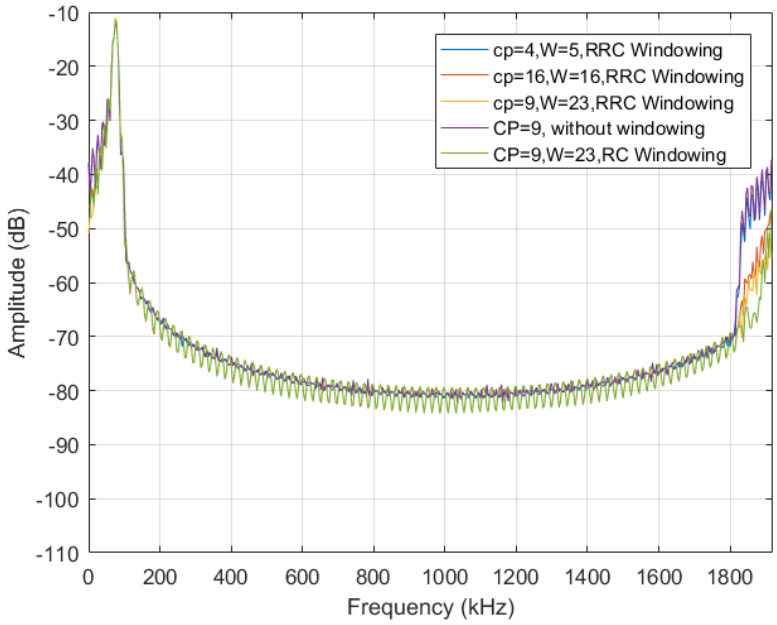

Figure 5-4 *Spectrum with different windowing configurations*

Here we test the transmitted signal spectra in different windowing and filtering configurations. The NB-IoT is close to the band edge without guard-band towards the first active LTE subcarrier. In these simulations linear PA is used. According to Figure 5-4 the interference leakage from NB-IoT to LTE on the transmitter side is effectively suppressed by filtering to a quite close level no matter the windowing configuration. On the other hand, the windowing has significant effect on the interference leakage within the NB-IoT band, which is not affected by filtering. Again, longer window transition interval is more effective. These results demonstrate that filtering and windowing both do have the capacity to suppression the sidelobes of NB-IoT signals, but they have different roles in the overall scheme.

5.1.5 Effect of Power Amplifier

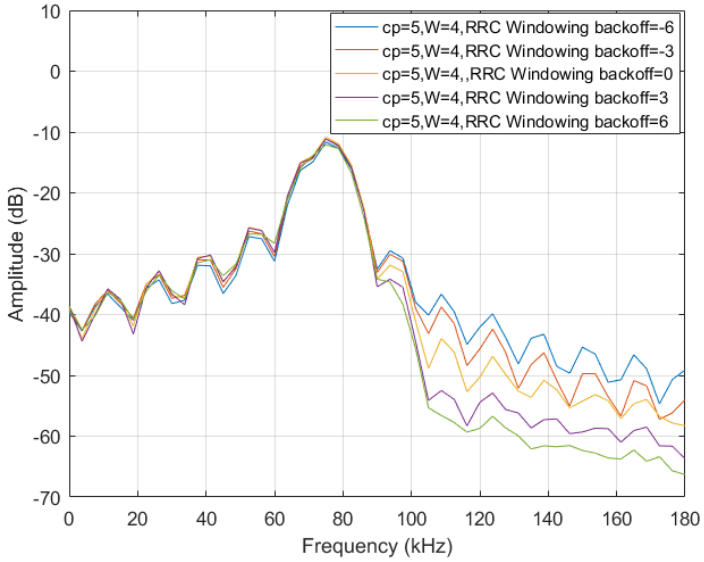

Figure 5-5 *Spectrum at PA output with different back-off values.*

The effects of power amplifier back-off is illustrated in Figure 5-5, reducing the back-off increases the spectral regrowth, as expected based on the discussion of Section 4.7

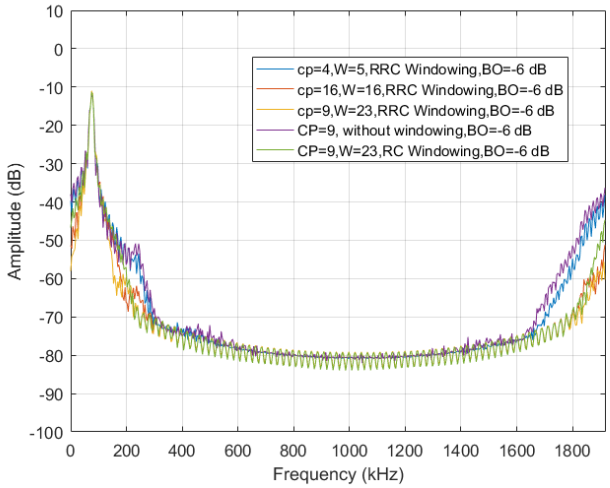

Figure 5-6 *Spectrum at PA output with different t windowing configurations*

As shown in Figure 5-6, the windowing approach with longer CP-extension has more effective in suppressing the spectral regrowth which is caused by PA's negative back-off. Some benefit for RRC-type constant envelope windowing can be seen

5.1.6 NB-IoT and LTE power levels in testing

During the simulation, both LTE/4QAM and LTE/64QAM are considered to indicate the effect of the LTE modulation scheme, especially the effect of the related signal power levels.

Generally, the target SINR in LTE depends on the used modulation and coding scheme. Using higher power doesn't essentially improve the link performance but increase interference to other users, thus reducing the system-level capacity. Here, relevant scenarios regarding to NB-IoT and LTE power levels are assumed in the simulations. The following three cases are considered:

- Optimum power level: NB-IoT and LTE subcarrier power level difference corresponding to optimum power level. To be more specific, considering the required SNR for BER=0.01, average NB-IoT subcarrier is 3.1 dB weaker than LTE/4QAM and 15.9 dB weaker than LTE/64QAM.
- NB-IoT critical power level: LTE signal 12 dB stronger than in optimum power level test. In this case, average NB-IoT subcarrier is 8.9 dB stronger than LTE/4QAM, but 3.9 dB weaker than LTE/64QAM.
- LTE critical power level: NB-IoT signal is 12 dB stronger than in optimum power level test. Opposite to LTE critical power level, average NB-IoT subcarrier is 15.2 dB weaker than LTE/4QAM and 27.9 dB weaker than LTE/64QAM.

5.2 Performance Analysis of NB-IoT without Guard Band

In this section, NB-IoT signal and LTE signal are transmitted without guard band. Transmission diagram is the same as Figure 5-1.In these simulations, the synchronicity is due to worst-case CFO of half subcarrier spacing and half of symbol duration for timing offset. Performance is then analyzed based on the simulation results.

5.2.1 NB-IoT critical Test case

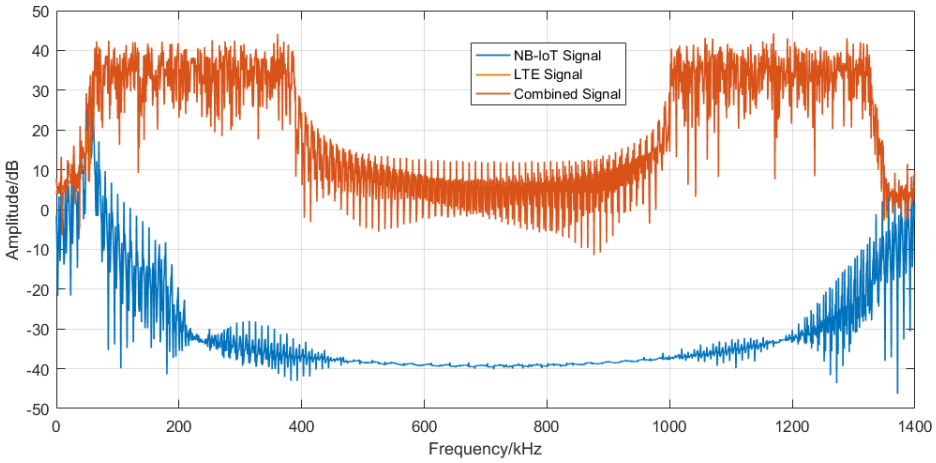

Figure 5-7 *Spectrum of transmitted signals in NB-IoT critical test*

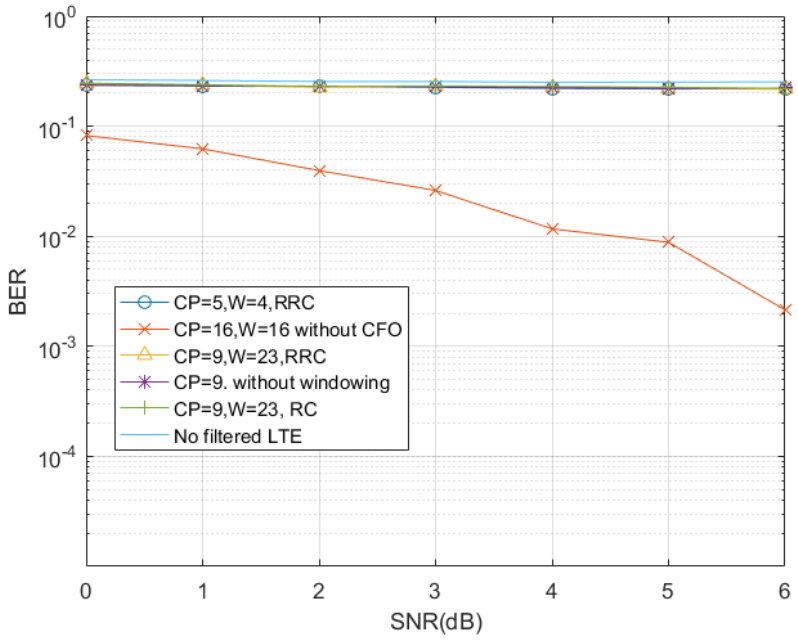

Figure 5-8 *BER NB-IoT performance in NB-IoT critical test case under asynchronous LTE/64QAM, BO= -6 dB， without guard-band*

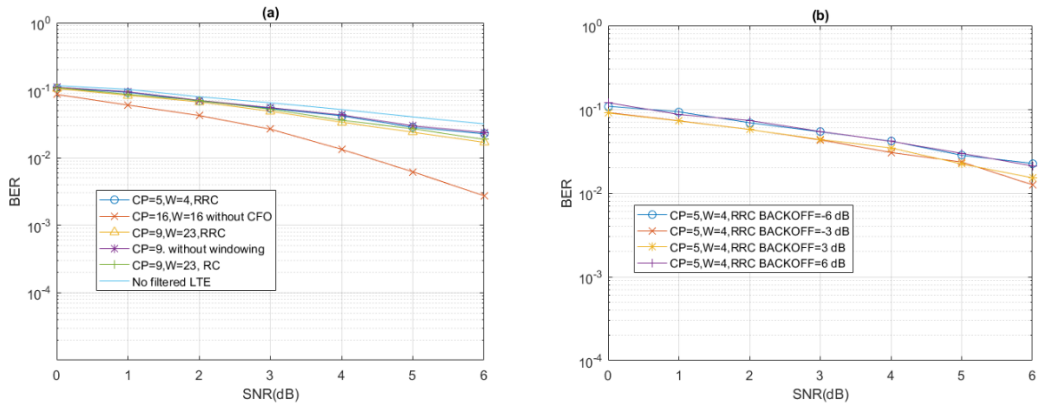

Figure 5-9 *BER for critical NB-IoT under asynchronous LTE/4QAM, without guard-band (a) Different windowing configurations with BO=-6 dB. (b) Different BOs*

The results are illustrated in Figure 5-8 and Figure 5-9. Due to the huge power level difference between LTE and NB-IoT signals, the performance of NB-IoT greatly degraded, even in the case of LTE/4QAM.

5.2.2 Optimum Power Test

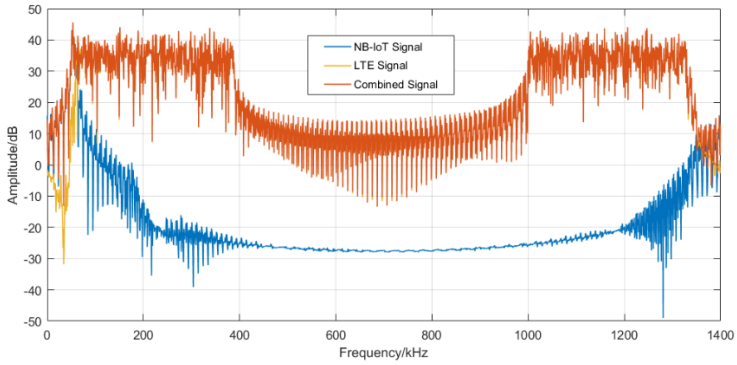

Figure 5-10 *Spectrum of transmitted signals in optimum power test*

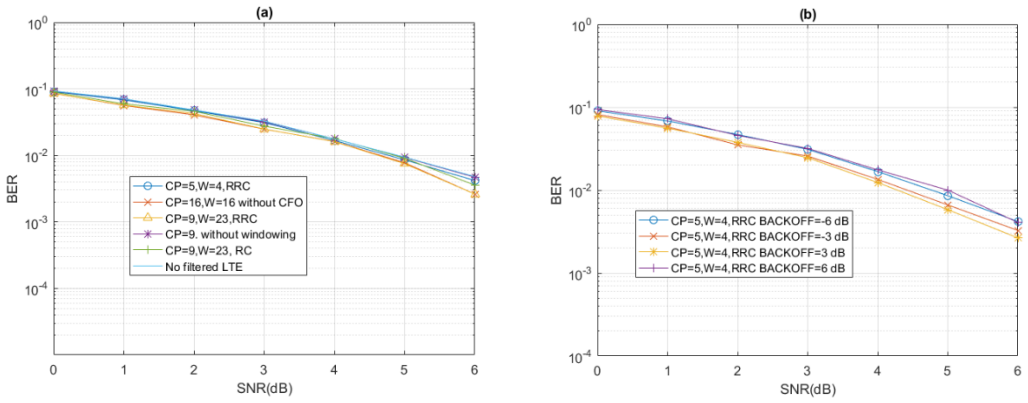

Figure 5-11 *BER for optimum power NB-IoT under asynchronous LTE/4QAM, without guard-band. (a) Different windowing configurations with BO=-6 dB. (b) Different BOs*

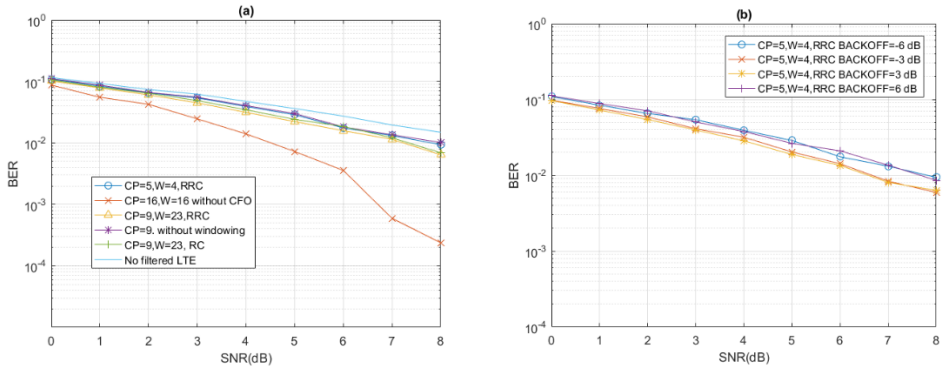

Figure 5-12 *BER for optimum NB-IoT power under asynchronous LTE/64QAM, without guard-band. (a) Different windowing configurations with BO=-6 dB. (b) Different BOs.*

The spectra of the transmitted signals are shown in Figure 5-10. In this case, average NB-IoT subcarrier is 15.9 dB weaker than LTE/64QAM modulated subcarriers, or 3.1 dB weaker than LTE/4QAM subcarriers. Both scenarios are simulated. Figure 5-11 (a) shows the performance of different windowing methods. During the simulation, LTE signal without filtering is also included to evaluate the effect of filtering on LTE power leakage. Although the windowing approach can decrease the sidelobe, depending on the length of CP and extension, the BER performance still shows only small differences. This is due to the filtering that minimizes the LTE sidelobes to approximately the same power level. However, with close observation, it can still be seen that windowing approach can slightly improve the interference mitigation.

Comparing Figure 5-11 (a) and Figure 5-12 (a), we see that NB-IoT is quite insensitive to LTE/4QAM at the optimum power level. However, since LTE/64QAM is transmitted at a considerably higher power level, it causes strong interference to NB-IoT in this scenario. The NB-IoT experiences about 3 dB loss at the 1 % BER level. From Figure 5-11(b) and Figure 5-12 (b), we see that the effect of power amplifier back-off. With LTE/4QAM, the SNR loss is reduced by about 0.7 dB, when the back-off is increased from -6 dB to 6 dB. In the case of LTE/64QAM the corresponding different is about 1.5 dB.

5.3 Performance Analysis of NB-IoT with One Subcarrier Guard Band

5.3.1 NB-IoT critical test case

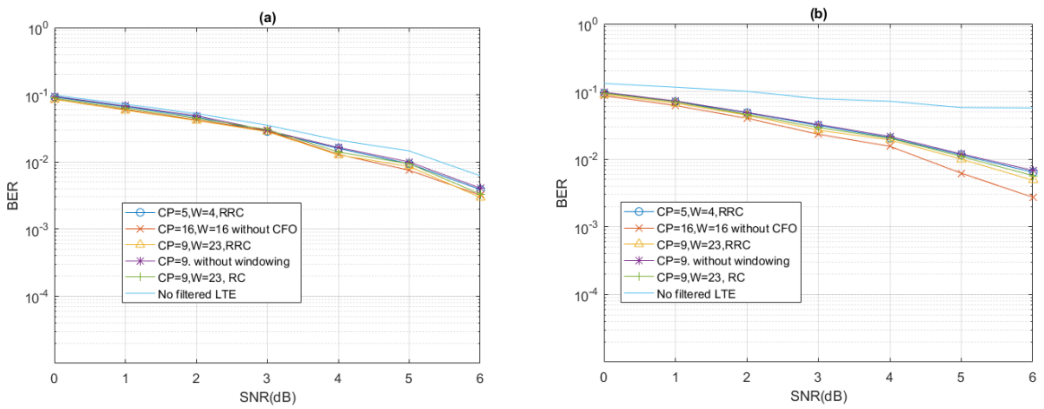

Figure 5-13 *BER for critical NB-IoT power level under asynchronous LTE with BO=-6 dB, with guard-band (a) LTE/4QAM (B) LTE/64QAM*

Under NB-IoT critical power testing with both LTE/4QAM and LTE/64QAM (Figure 5-13), the performance is quite acceptable with all windowing schemes, and also without windowing. In the LTE/64QAM case, the performance loss is more than about 0.5 dB. We also notice that in these cases, the benefit from filtering in the LTE transmitter is significant.

5.3.2 Optimum Power Test Cases

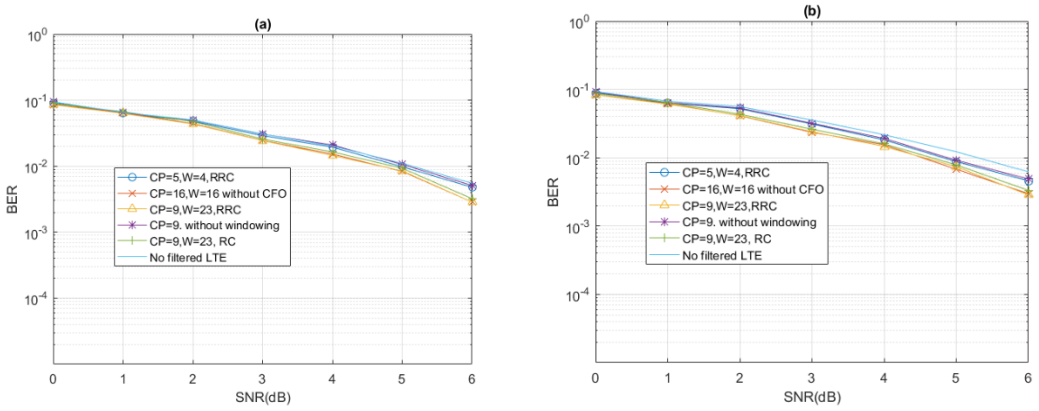

Figure 5-14 *BER for optimum NB-IoT power level under asynchronous LTE, with guard-band, BO=-6 dB. (a) LTE/4QAM (b) LTE/64QAM*

With optimum power testing, the NB-IoT signal performs properly with both LTE/4QAM and LTE/64QAM. Also in this case, the differences between windowing schemes are marginal.

5.4 Performance Analysis of LTE without Guard Band

In this simulation, NB-IoT signal and LTE signal are transmitted without guard band. Transmission diagram is same as Figure 5-2. Performance is then analyzed based on simulation results. Worst-case CFO and TOF is the cause of asynchronous operation also in these simulations.

5.4.1 Optimum Power Test cases:

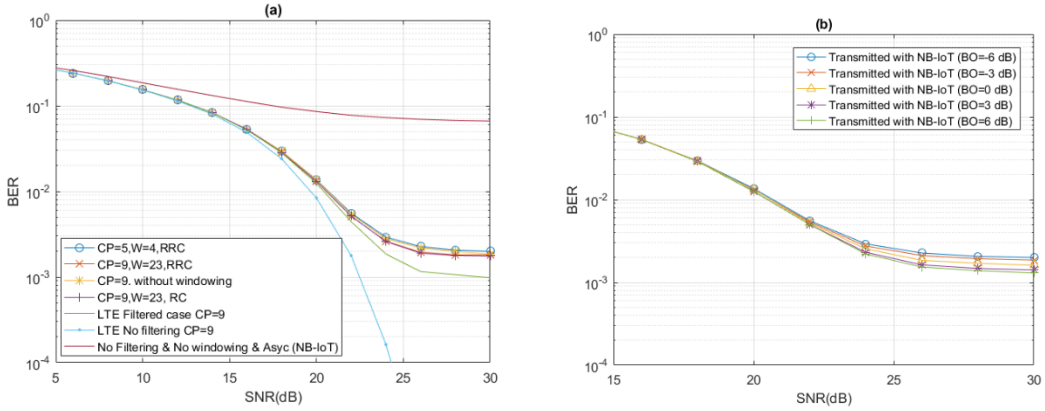

Figure 5-15 *BER for optimum power testing for LTE/64QAM under asynchronous NB-IoT, without guard-band (a) Different windowing configuration with BO=-6 dB (b) Different BOs*

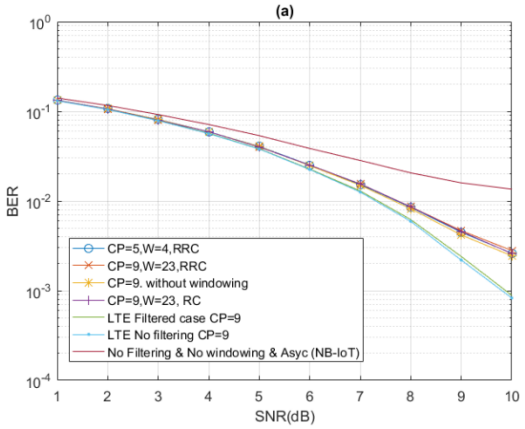

Figure 5-16 *BER for Optimum power testing for LTE/4QAM under asynchronous NB-IoT, without guard-band*

For 4QAM-LTE signal, the interference introduced by NB-IoT is acceptable less than 0.5 dB, if filtering is applied. We can also see that the used LTE filtering has minor effect on the LTE/4QAM performance in the synchronous case. With LTE/64QAM, the performance loss is about 1.5 dB at the 1 % BER level, but this can still be considered acceptable. In this case, LTE filtering introduce almost similar loss even with synchronous transmission. The difference between NB-IoT windowing schemes are marginal and also the NB-IoT transmitter's back-off has only a relatively small effect.

5.4.2 LTE Critical Testing

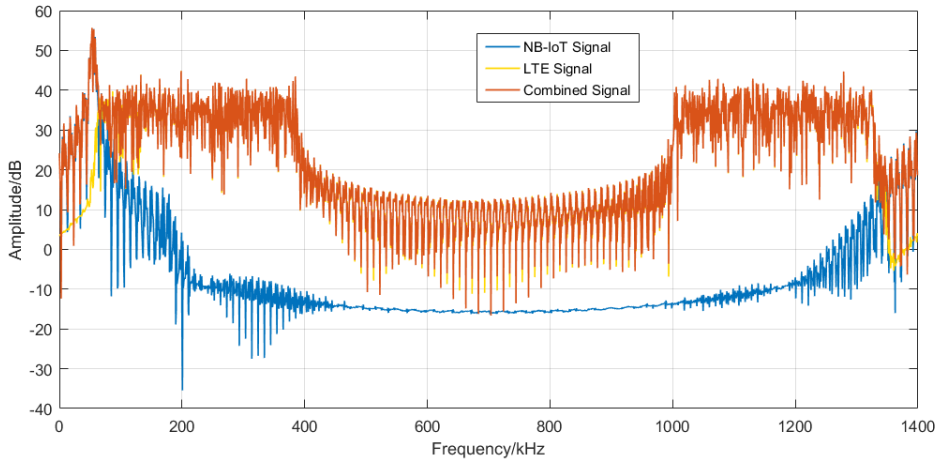

Figure 5-17 *Spectrum of transmitted signals in the LTE critical test*

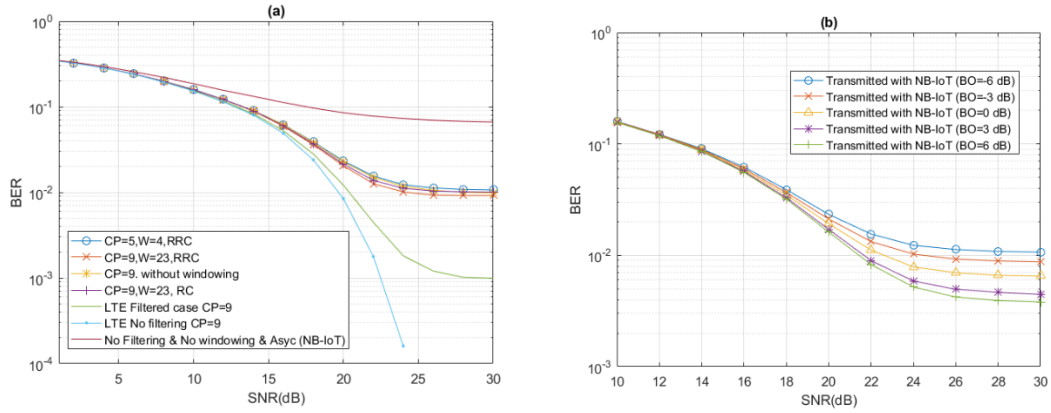

Figure 5-18 *BER for LTE/64QAM critical testing under asynchronous NB-IoT, without guard-band. (a) Different windowing configuration BO=-6 dB. (b)Different BOs*

In LTE critical testing case, the power level of NB-IoT is 12 dB stronger than optimum QPSK-LTE. Thus, average NB-IoT subcarrier is 8.9 dB stronger than LTE/4QAM subcarriers and 3.9 dB weaker than LTE/64QAM subcarriers.

Even though filtering significantly reduces interference leakage from NB-IoT to LTE, the performance in this scenario cannot be considered acceptable, as the SNR loss exceeds 1.5 dB with 4QAM and 2 dB with 64QAM at 1% BER with high back-off. In this case, the NB-IoT back-off has significant effect, and with small back-offs the performance loss becomes much higher..

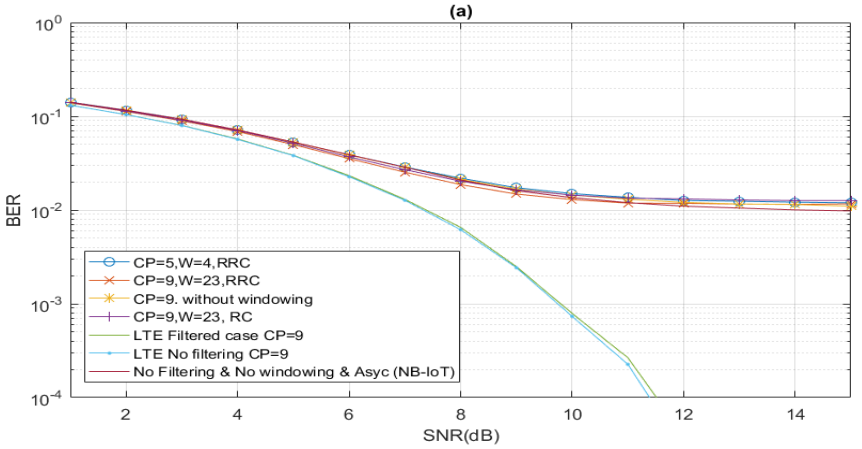

Figure 5-19 *BER for LTE critical testing for LTE/4QAM under asynchronous NB-IoT, without guard-band, BO= -6 dB*

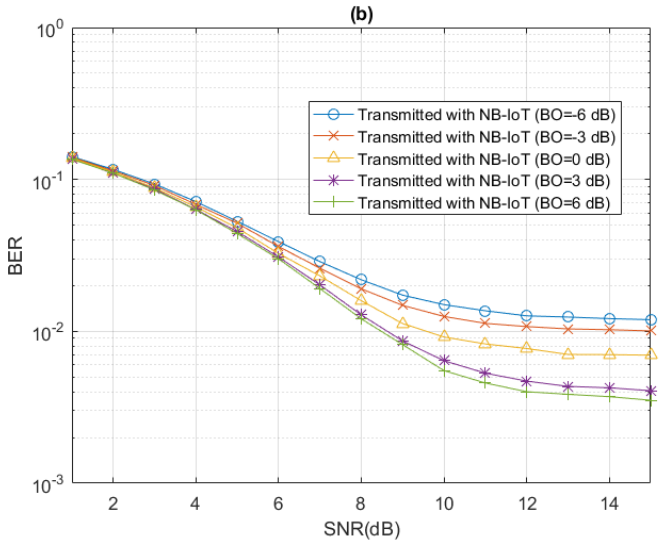

Figure 5-20 *BER for LTE critical testing for LTE/4QAM under asynchronous NB-IoT, without guard-band, different BOs*

5.5 Performance Analysis of LTE with One Subcarrier Guard Band

5.5.1 Optimum Power Level Test

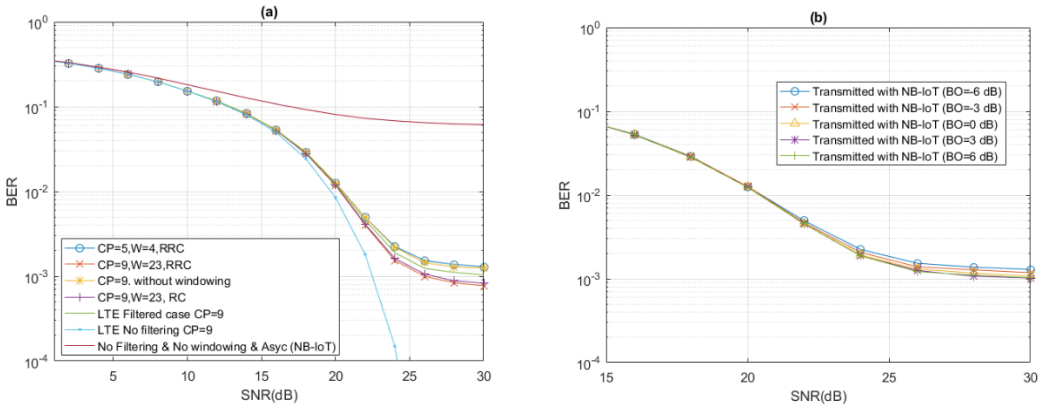

Figure 5-21 *BER for optimum power testing for LTE/64QAM under asynchronous NB-IoT, with guard-band. (a) Different windowing configuration BO=-6 dB. (b) Different BOs*

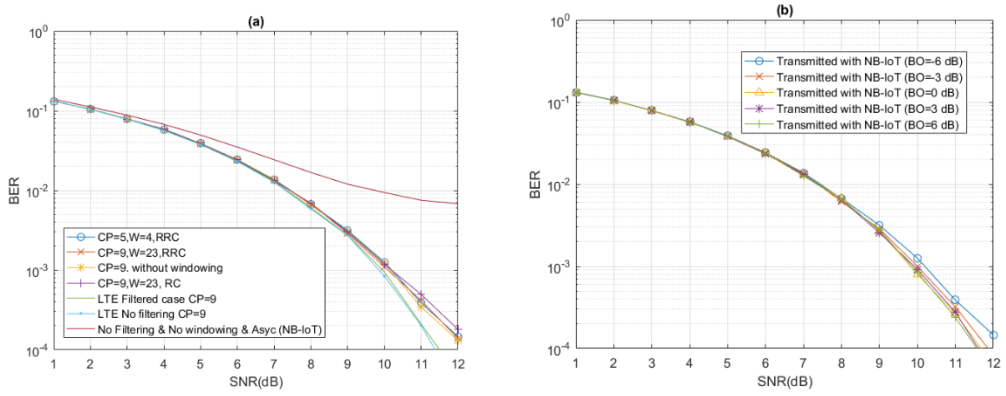

Figure 5-22 *BER for optimum power testing for LTE/4QAM under asynchronous NB-IoT. (a) Different windowing configuration BO=-6 dB, (b) Different BOs*

Once one subcarrier guard band is introduced, the BER performance for both 4QAM-LTE and LTE/64QAM is quite good and acceptable. Interference suppression by filtering is essential, but the differences between different windowing schemes can be considered marginal. We can also observe from Figure 5-21 (b) and Figure 5-22 (b) that the NB-IoT PA nonlinearity does not affect much the interference leakage to LTE.

5.5.2 LTE CRITICAL POWER TEST

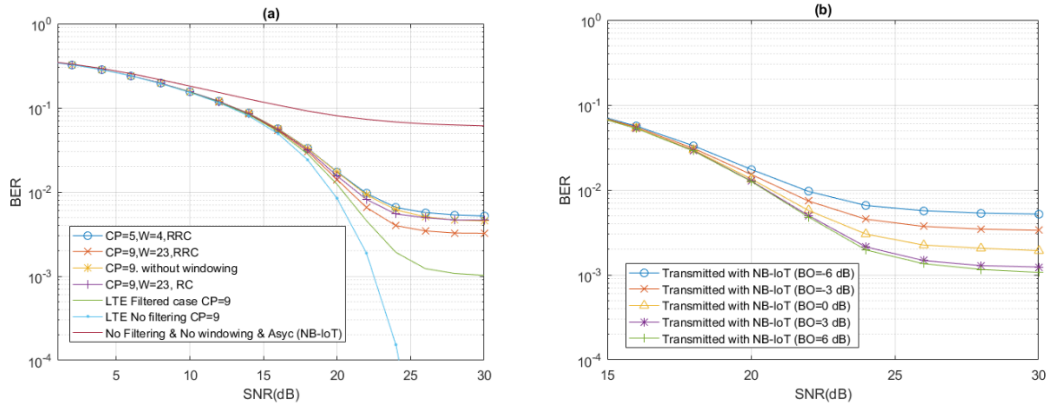

Figure 5-23 *BER for LTE critical testing for LTE/64QAM under asynchronous NB-IoT, with guard-band (a) different windowing configuration BO=-6 dB (B) different BO*

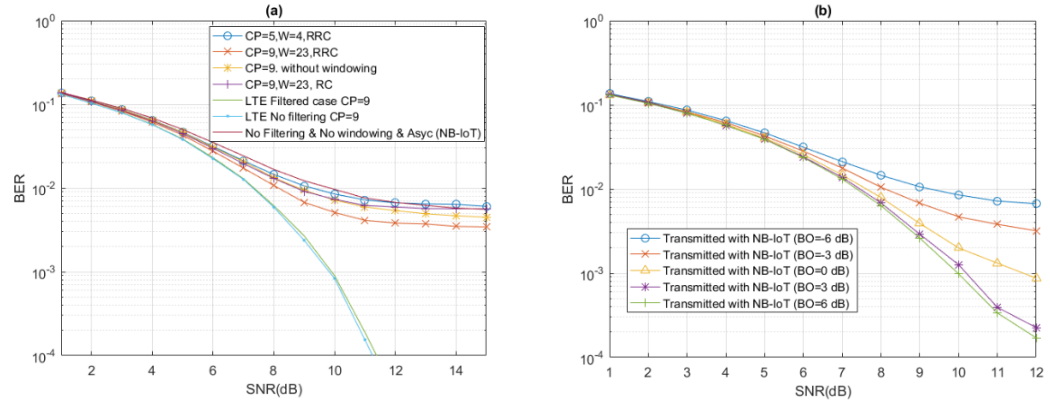

Figure 5-24 *BER for LTE critical testing for LTE/4QAM under asynchronous NB-IoT, with guard-band (a) different windowing configuration BO=-6 dB (B) different BO*

With LTE critical power testing, the benefits of windowing are significant and also some advantage for the RRC-type constant-envelope windowing with longer transition interval can be seen. As for the nonlinearity of NB-IoT device's PA, its effect is illustrated in Figure 5-23 (b) and Figure 5-24 (b). It can be concluded that the effect is significant, Improper back-off value could distortion the signal or resulting spectrum regrowth. Basically, with long window and non-negative back-off, the performance can be found to be quite acceptable with both LTE/4QAM and LTE/64QAM..

6. CONCLUSION

The main objective of this thesis was achieved by evaluating the interference from single-tone NB-IoT to LTE, and vice versa, in case of asynchronous uplink transmission scenarios caused by worst-case carrier frequency offset and half symbol duration timing offset between LTE and NB-IoT. Our basic waveform choice is filtered OFDM, which is the more powerful spectrum enhancement method considered in the 5G system standardization in 3GPP, in comparison with time-domain windowing. With the implementation of filtering for both NB-IoT and LTE sub-bands, out-of-band interference in both directions can be effectively suppressed. Here it is important to select properly the filtering transition bands. The designed filters were found to cause only minor degradation in the synchronized scenario. Also, time-domain windowing was introduced to further suppress the sidelobes of NB-IoT. The simulation results show that in critical scenarios, longer CP-extension provides clearly better performance than a shorter CP-extension. While the extended CP mode is seldom used in LTE, 5G will support so-called mixed numerology, e.g., using different subcarrier spacings in different sub-bands of the same carrier. Then it also becomes possible the use of extended CP for NB-IoT while other services are operating with the normal CP length.

The BER performance analysis of Chapter 5 indicates that 1-subcarrier guard-band between single-tone NB-IoT and LTE resource blocks helps to effectively reduce the critical interference leakage from NB-IoT to LTE. With such guard-band, the LTE performance was found to be quite acceptable (less than 1 dB SNR degradation) also in the test cases with LTE-critical power levels. Time-domain windowing with longer CP-extension contributes significantly to reaching this target, and also NB-IoT transmitter's back-off should take at least positive values in the Rapp model. Without guard-band, the LTE performance is still acceptable with the optimal power levels of NB-IoT and LTE, but t in the LTE critical test cases, only marginally acceptable performance was achieved. And also the NB-IoT back-off is in a critical role. This indicating the importance of good power control for single-tone NB-IoT when it is operating at the edge of NB-IoT resource block.

Regarding the interference from LTE to NB-IoT, the performance is quite acceptable with optimal power levels, except for the case of LTE/64QAM without guard-band,

where the SNR loss is higher (about 2 dB at 1 % BER). In the NB-IoT critical test cases, good performance is achieved with 1-subcarrier guard-band. While without a guard-band the performance is only marginally acceptable with 4QAM (about 2 dB SNR loss at 1% BER), but quite poor with 64QAM. It can be concluded that effective power control for single-tone NB-IoT is necessary when the tone is at the edge of the NB-IoT resource block. On the other hand, NB-IoT is able to operate with very low SNR, while the test cases in our study are based on the LTE's SNR requirement for binary PSK. Therefore, the strong error control coding of NB-IoT could allow its operation also in NB-IoT critical test cases, with reduced data rates. Time-domain windowing doesn't have much effect on the interference leakage from LTE to NB-IoT, as could be expected. However, it could be essential for reducing the interference between asynchronous IoT users, and this is an important topic for future studies.

With optimal power levels, both LTE and NB-IoT performances are not critically affected by the nonlinearity of the NB-IoT transmitter's power amplifier, but with higher power levels of NB-IoT, better linearity becomes essential. Also time-domain windowing with longer transition interval allows the NB-IoT to operate at higher power levels without critical interference to LTE, thus relaxing the power control requirements.

REFERENCES

[1] Beyene Y D, Jantti R, Tirkkonen O, et al. NB-IoT technology overview and experience from cloud-RAN implementation[J]. IEEE Wireless Communications, 2017, 24(3): 26-32.

[2] Loulou A E Y M. Enhanced OFDM for fragmented spectrum use[J]. 2013.

[3] Mahmoud H A, Arslan H. Sidelobe suppression in OFDM-based spectrum sharing systems using adaptive symbol transition[J]. IEEE communications letters, 2008, 12(2).

[4] Luo J, Kortke A, Keusgen W. Guardband optimization for cellular systems applying raised cosine windowed OFDM[J]. Wireless personal communications, 2014, 78(2): 1375-1390.

[5] Brandes S, Cosovic I, Schnell M. Reduction of out-of-band radiation in OFDM systems by insertion of cancellation carriers[J]. IEEE communications letters, 2006, 10(6): 420-422.

[6] Cosovic I, Brandes S, Schnell M. Subcarrier weighting: a method for sidelobe suppression in OFDM systems[J]. IEEE Communications Letters, 2006, 10(6): 444-446.

[7] Cosovic I, Mazzoni T. Suppression of sidelobes in OFDM systems by multiple-choice sequences[J]. Transactions on Emerging Telecommunications Technologies, 2006, 17(6): 623-630.

[8] Mahmoud H A, Arslan H. Sidelobe suppression in OFDM-based spectrum sharing systems using adaptive symbol transition[J]. IEEE communications letters, 2008, 12(2).

[9] Loulou A E, Renfors M. Enhanced OFDM for fragmented spectrum use in 5G systems[J]. Transactions on Emerging Telecommunications Technologies, 2015, 26(1): 31-45.

[10] Shafi M, Molisch A F, Smith P J, et al. 5G: A Tutorial Overview of Standards, Trials, Challenges, Deployment, and Practice[J]. IEEE Journal on Selected Areas in Communications, 2017, 35(6): 1201-1221.

[11] Marcus M J. 5G and" IMT for 2020 and beyond"[Spectrum Policy and Regulatory Issues][J]. IEEE Wireless Communications, 2015, 22(4): 2-3.

[12] Minimum Requirements Related to Technical Performance for IMT-2020 Radio Interface(s), document ITU-R M.[IMT-2020.TECH PERFREQ], Oct. 2016.

[13] Simsek M, Aijaz A, Dohler M, et al. 5G-enabled tactile internet[J]. IEEE Journal on Selected Areas in Communications, 2016, 34(3): 460-473.

[14] Cardona N. Scientific Challenges Towards 5G Mobile Communications[J]. COST IC1004 White paper, Tech. Rep, 2013.

[15] Ericsson, "Cellular Networks for Massive IoT-Enabling Low Power Wide Area Applications," white paper, 2016; https://www.ericsson.com/res/docs/white-papers/wp_iot.pdf

[16] 3GPP, New Work Item: NarrowBand IOT (NB-IOT), TSG RAN Meeting #69, 2015; http://www.3gpp.org/FTP/tsg_ ran/TSG_RAN/TSGR 69/Docs/RP-151621.zip

[17] 3GPP TS 36.331, "Evolved Universal Terrestrial Radio Access (E-UTRA); Resource Control (RRC) Protocol Specification (Release 13)," 2016; http://www.3gpp.org/ftp/Specs/archi ve/36series/36.331/36331-d20.zip.

[18] HUAWEI, "NB-IoT-Enabling New Business Opportunities," 2015; http://www.huawei.com/minisite/4-5g/img/NB-IOT.pdf

[19] Osseiran A, Boccardi F, Braun V, et al. Scenarios for 5G mobile and wireless communications: the vision of the METIS project[J]. IEEE Communications Magazine, 2014, 52(5): 26-35.

[20] Hara S, Prasad R. Multicarrier techniques for 4G mobile communications[M]. Artech House, 2003.

[21] Palattella M R, Dohler M, Grieco A, et al. Internet of things in the 5G era: Enablers, architecture, and business models[J]. IEEE Journal on Selected Areas in Communications, 2016, 34(3): 510-527.

[22] Lutfi S. Phase Noise Estimation and Mitigation in Uplink OFDMA[J]. 2013.

[23] Osesina O I, Zhang Y, Pagoti S. OFDM Carrier Frequency Offset Estimation[J]. 2006.

[24] Chen B, Wang H. Maximum likelihood estimation of OFDM carrier frequency offset[C]//Communications, 2002. ICC 2002. IEEE International Conference on. IEEE, 2002, 1: 49-53.

[25] Fang S H, Chen J Y, Shieh M D, et al. Subspace-based blind channel estimation for OFDM systems with conjugate-symmetric property[C]//Vehicular Technology Conference (VTC 2010-Spring), 2010 IEEE 71st. IEEE, 2010: 1-5.

[26] Yadav A, Tapio V, Juntti M, et al. Timing and frequency offsets compensation in relay transmission for 3GPP LTE uplink[C]//Communications (ICC), 2010 IEEE International Conference on. IEEE, 2010: 1-6.

[27] Jha U S, Prasad R. OFDM towards fixed and mobile broadband wireless access[M]. Artech House, Inc., 2007.

[28] Tandiya N. Constant-Envelope Modulation Schemes with Turbo Coding[M]. University of California, Irvine, 2015.

[29] Weiss T, Hillenbrand J, Krohn A, et al. Mutual interference in OFDM-based spectrum pooling systems[C]//Vehicular Technology Conference, 2004. VTC 2004-Spring. 2004 IEEE 59th. IEEE, 2004, 4: 1873-1877.

[30] Beaulieu N C, Tan P. On the effects of receiver windowing on OFDM performance in the presence of carrier frequency offset[J]. IEEE Transactions on Wireless Communications, 2007, 6(1).

[31] Shabany M, Gulak P G. Efficient compensation of the nonlinearity of solid-state power amplifiers using adaptive sequential Monte Carlo methods[J]. IEEE Transactions on Circuits and Systems I: Regular Papers, 2008, 55(10): 3270-3283.

[32] Drotar P, Gazda J, Deumal M, et al. Receiver based compensation of nonlinear distortion in MIMO-OFDM[C]//RF Front-ends for Software Defined and Cognitive Radio Solutions (IMWS), 2010 IEEE International Microwave Workshop Series on. IEEE, 2010: 1-4.

[33] Saleh A A M. Frequency-independent and frequency-dependent nonlinear models of TWT amplifiers[J]. IEEE Transactions on communications, 1981, 29(11): 1715-1720.

[34] Rapp C. Effects of HPA-nonlinearity on a 4-DPSK/OFDM-signal for a digital sound broadcasting signal[C]//In ESA, Second European Conference on Satellite Communications (ECSC-2) p 179-184 (SEE N92-15210 06-32). 1991.